INTEGRATIVE CLICK CHEMISTRIES FOR TUNING PHYSICOCHEMICAL PROPERTIES OF CANCER CELL-LADEN HYDROGELS

A Thesis

Submitted to the Faculty

of

Purdue University

by

Hunter C. Johnson

In Partial Fulfillment of the

Requirements for the Degree

of

Master of Science in Biomedical Engineering

May 2020

Purdue University

Indianapolis, Indiana

THE PURDUE UNIVERSITY GRADUATE SCHOOL
STATEMENT OF THESIS APPROVAL

Dr.Chien-Chi Lin, Chair

Department of Biomedical Engineering

Dr. Sungsoo Na

Department of Biomedical Engineering

Dr. Christoph Naumann

Department of Chemistry and Chemical Biology

Approved by:

Dr. Julie Ji

Head of the Graduate Program

This is for my Father.

ACKNOWLEDGMENTS

I would like to thank my advisor Dr. Chien-Chi Lin for the opportunity to conduct research under his supervision. I have gained invaluable insight into many communication and research related matters under his leadership.

I would also like to thank my committee members Dr. Sungsoo Na and Dr. Christoph Naumann.

A heart-felt and sincere thank you goes to Mrs. Sherry Clemens for all of her administrative guidance and facilitation over the course of several years.

Additionally, I would like to thank all of the lab members (present and past): Dr. Hung-Yi (Gino) Liu, Dr. Min-Hee Kim, Dr. Fang-Yi Lin, Matt Arkenburg, Chun-Yi (Wilbert) Chang, Dustin Moore, Kevin Peuler, Han Nguyen, and Nathan Dimmitt who have helped me throughout this journey and become an unforgettable part of my life.

Lastly, I would like to thank my grandmother, Wilma MacDonald, and my dear friends, Richard Hamblin and Robert Lee, for their continued love, motivation and support throughout many of the ups and downs of life.

TABLE OF CONTENTS

Page

LIST OF FIGURES

Figure Page

Figure Page

LIST OF SYMBOLS

G'	shear modulus
G"	storage modulus
M	molar
R	molar ratio of thiol to norbornene
Q	molar ratio of aldehyde to carbohydrazide

LIST OF ABBREVIATIONS

αSMA	α smooth muscle actin
3D	three-dimensional
BSA	bovine serum albumin
CSCs	cancer stem cells
CA	carbic anhydride
CDH	carbohydrazide
CD44	cluster of differentiation 44
DAPI	4',6'-diamidino-2-phenylindole
DIEA	N,N-diisopropylethylamine
DMEM	Dulbecco's modified eagle's medium
DMF	dimethyformamide
DMMB	1,9-dimethyl-methylene blue
DMSO	dimethyl sulfoxide
DPBS	Dulbecco's phosphate-buffered saline
EDC	1-ethyl-3-(3-dimethylaminopropyl)carbodiimide HCl
EMT	epithelial-mesenchymal transition
ECM	extracellular matrix
FBS	fetal bovine serum
Gel(B)NB	type B gelatin norbornene
GEM	gemcitabine
GFOFER	glycine-phenylalanine-hydroxyproline-glycine-glutamicacid-arginine
HA	hyaluronan or hyaluronic acid
HA-Tz	tetrazinated hyaluronic acid

HATU	1-[Bis(dimethylamino)methylene]-1H-1,2,3-triazolo[4,5-b]pyridinium 3-oxide hexafluorophosphate
Hep-Tz	tetrazinated heparin
hMSCs	human mesenchymal stem cells
HOBt	hydroxy benzotriazole
iEDDA	inverse electron Diels-Alder addition
LAP	lithium phenyl-2,4,6-trimethylbenzoylphosphinate
LD50	lethal dose, 50%
LMWoHA	low molecular weight oxidized hyaluronic acid
Me-HA	methacrylated hyaluronic acid
MMP	matrix metalloproteinase
MMWoHA	medium molecular weight oxidized hyaluronic acid
MTT	3-(4,5-dimethylthiazol-2-yl)-2,5-diphenyltetrazolium bromide
MT	mushroom tyrosinase
MW	molecular weight
MWCO	molecular weight cut-off
NB	norbornene
NHS	N-hydroxysuccinimide
oDex	oxidized dextran
oHA	oxidized hyaluronic acid
PAA	polyacrylamide
PanIN	pancreatic intraepithelial neoplasia
PBS	phosphate-buffered saline
PDAC	pancreatic ductal adenocarcinoma
PEG	poly(ethylene glycol)
PEG4pAld	4-arm PEG-propionaldehyde
PEG4SH	4-arm PEG-thiol
PEG4Tz	4-arm PEG-tetrazine
PEG8NB	8-arm PEG-norbornene

PSCs	pancreatic stellate cells
RHAMM	receptor for hyaluronic acid-mediated motility
RGD	arginine-glycine-aspartic acid
RM	regular media
SH	thiol
SM	spheroid media
TMMs	tetrazine-modified macromers
TNBSA	2,4,5-trinitrobenzene sulfonic acid
Tz	tetrazine
Tz-amine	tetrazine-amine
TCPs	tissue culture plastics
TCO	trans-cyclooctyne
TME	tumor microenvironment
VICs	valvular interstitial cells

ABSTRACT

Johnson, Hunter C. M.S.B.M.E., Purdue University, May 2020. Integrative Click Chemistries for Tuning Physicochemical Properties of Cancer Cell-Laden Hydrogels. Major Professor: Chien-Chi Lin.

The pancreas is a vital organ that secretes key metabolic hormones and digestive enzymes. In pancreatic ductal adenocarcinoma (PDAC), one of the leading causes of cancer-related death in the world, limited advances in diagnosis or therapies have been made over decades. Key features of PDAC progression include an elevated matrix stiffness and an increased deposition of extracellular matrices (ECM), such as hyaluronic acid (HA). Understanding how cells interact with components in the tumor microenvironment (TME) as PDAC progresses can assist in developing diagnostic tools and therapeutic treatment options. In recent years, hydrogels have proven to be an excellent platform for studying cell-cell and cell-matrix interactions. Utilizing chemically modified and naturally derived materials, hydrogel networks can be formed to encompass not only the components, but also the physicochemical properties of the dynamic TME. In this work, a dynamic hydrogel system that integrates multiple click chemistries was developed for tuning matrix physicochemical properties in a manner similar to the temporally increased matrix stiffness and depositions of HA. Subsequently, these dynamic hydrogels were used to investigate how matrix stiffening and increased HA presentation might affect survival of PDAC cells and their response to chemotherapeutics.

1. INTRODUCTION

1.1 The pancreas and PDAC

The pancreas plays a vital role in energy consumption and regulation of metabolism [1]. It consists of two functionally and morphologically distinct components, namely, the exocrine and endocrine pancreas [1]. The exocrine tissues are made up of acinar and ductal cells, of which the acinar cells produce digestive enzymes and release them into pancreatic ducts [1]. The endocrine tissues are comprised of cells that produce and secrete specific hormones responsible for regulation of blood glucose levels [1]. PDAC and diabetes are two of the most common and devastating diseases associated with the exocrine and endocrine pancreas, respectively [1]. After cardiovascular diseases, cancers are the second-most leading cause of death in America [2]. Of the estimated 57,770 new pancreatic cancer incidences in 2019, there is an estimated 45,750 deaths [2]. Pancreatic cancer incidences accounted for 3% of the total incidences in 2019, while the associated deaths were 7 and 8% for male and female patients, respectively [2]. The incidence rates for pancreatic cancers continue to increase, while the survival rates are among the lowest of all cancers [2].

1.1.1 Treatments of PDAC

Therapeutic failures can be attributed to the PDAC microenvironment, which is regulated by not only the tumor cells, but also cells in the stromal tissue, including pancreatic stellate cells, myofibroblasts, inflammatory fibroblasts, and immune cells [3]. Additionally, the cell-type of origin dictates the phenotype of the tumor [4]. For example, when tumors originate from ductal cells, high-grade pancreatic intraepithelial neoplasia (PanIN) lesion growth is accelerated when compared to tumors orig-

inating from acinar cells, in which metaplasia and low-grade PanIN lesions are more common [4]. Furthermore, differing biologies result in cells with varied innate epithelial or mesenchymal characteristics [5]. Small molecules, such as non-coding RNA and micro RNA, also play a significant role in PDAC chemoresistance, as well as overexpression of integrins that regulate cellular functions such as epithelial-mesenchymal transition (EMT) [6].

The current standard-of-care for early-stage PDAC is curative-intended resection and adjuvant therapy [7]. while the standard-of-care for advanced-stage and palliative treatment of PDAC is gemcitabine (GEM) [8, 9]. In other gastrointestinal tract cancers, such as esophagus and gastric cancer, neoadjuvant therapies and perioperative multimodal therapies have significantly improved the outcome of patients with resectable tumors; thus, these therapies may prove beneficial in the treatment of PDAC [7]. Another treatment option for resectable tumors, for BRCA-positive PDAC, is poly-ADP-ribose polymerase inhibitors [10]. Unfortunately, early diagnoses and treatment is unlikely as only 10-15% of patients are diagnosed when the tumor is resectable [9]. Therefore, there is a need to establish greater understanding of the progression of PDAC, namely, through the interactions of cells with other cells and cells with their changing environment for improved diagnostic and even therapeutic tools.

1.1.2 Extracellular matrix (ECM) of PDAC

The ECM is a three-dimensional (3D) network of highly dynamic and heterogeneous biomolecules that regulate many cellular functions, including migration, spreading, differentiation, and proliferation [11, 12]. Dysregulation of ECM remodeling can result in structural, compositional, and functional defects that eventually lead to pathological events such as fibrosis and invasive cancers [11]. In recent years, biomimetic materials have enabled the recapitulation of critical ECM properties (e.g., stiffness and cell adhesion sites) in vitro. Certain integrin ligands, such as fibronectin

derived arginine-glycine-aspartic acid (RGD), provide the ability for cell attachment [13, 14] while other motifs (e.g., glycine-phenylalanine-hydroxyproline-glycine-glutamic acid-arginine; GFOGER) direct cellular differentiation [13]. In addition to biochemical cues, biophysical properties of ECM (e.g., stiffness, stress-relaxation) also regulate stem cell phenotype and fate [15]. For example, it was discovered that matrix stress-relaxation promote spreading and differentiation of mesenchymal stem cells [16].

1.1.3 Mechanics of PDAC stromal tissues

Pancreatic cancer is among the stiffest solid carcinomas in humans marked with an extraordinary desmoplastic reaction [17]. Increases in collagen-I deposition and fiber thickness, by cells such as cancer associated fibroblasts and activated pancreatic stellate cells (PSCs), promote cell survival, proliferation and migration [17, 18]. Additionally, alignment of collagen-I fibers lead to increases in matrix stiffness, which potentially leads to increased metastatic characteristics [17]. The stiffness of healthy pancreatic tissue, PanIN, and PDAC, as well as several PDAC cell lines, were determined via atomic force microscopy as shown in Figure 1.1. Another consequence of the dense stroma is the abundance of various ECM molecules and their ability to retain water, which increases interstitial fluid pressure [18]. All of these factors are believed to promote EMT and increased drug resistance [17, 18].

1.1.4 Biochemical compositions of PDAC stromal tissue

Tumor-derived ECM is biochemically distinct from and typically stiffer than ECM in healthy tissue [17, 20]. The altered state of the ECM creates a niche for cancer stem cells (CSCs), which have self-renewing capabilities, tumor-initiating capacities, and increased chemoresistance [20]. Depending on the cell of origin [4] and the biology of the patient (e.g. increased or decreased presence of cell-surface proteins relevant to disease progression) [5], tumors display varied phenotypes, including their

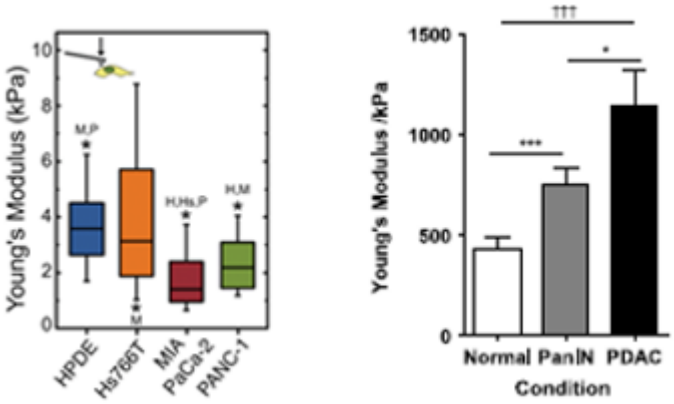

Fig. 1.1. (left) PDAC cell stiffness [19] and (right) pancreatic tissue stiffness from healthy to diseased states [17]

innate epithelial or mesenchymal characteristics. Variables such as matrix stiffness and quantities of cell-surface proteins and extracellular matrix components result in increased chemoresistance of PDAC tumors, making them increasingly difficult to treat [6].

Recently, it is suggested that hyaluronan (HA), a linear glycosaminoglycan present in the majority of tissues, creates a favorable environment for cancer progression [21]. For example, when HA binds to cluster of differentiation 44 (CD44), multiple receptor kinases are stimulated in HCT116 colon cancer cells, which leads to increased cell adhesion, proliferation, invasion, and overall survival [22]. HA also binds to toll like receptor 4, which promotes epithelial repair in radiation injury models and mediates normal growth of epithelial stem cells in the colon and intestine [22]. HA also binds to receptor for HA-mediated motility (RHAMM) [21]. HA binding to CD44 and RHAMM mediates cellular processes such as cell adhesion, migration, and survival [21]. RHAMM and CD44 also function as co-receptors for activating transmembrane tyrosine kinases [21]. PDAC is characterized by dense desmoplastic stroma and increased accumulation of HA (Figure 1.2). Increased HA presence correlates to poor prognosis in PDAC mouse models [21]. An upregulation of secreted HA synthases, through tumor-stromal cell interactions, results in an increased abundance of HA in

PDAC and this contributes to many malignant characteristics such as unregulated proliferation, migration, invasion and angiogenesis [20, 22]. This abundance of HA also could act as a physical barrier through sheer amount of the molecule and its ability to retain water, increasing interstitial fluid pressure, decreasing the efficacy of chemotherapeutics [18, 20]. Therefore, blocking HA-initiated signaling could facilitate therapies for PDAC by reducing malignant characteristics. This approach has been attempted in colon cancer, where HA-binding interactions were blocked with a 12-mer peptide [21].

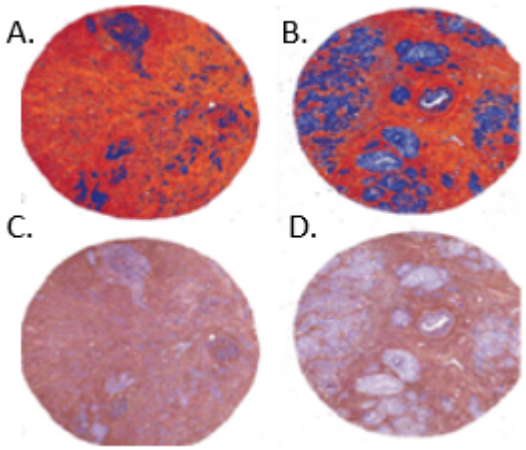

Fig. 1.2. (A, B) IHC staining (red) of overexpressed HA in pancreatic tumors; (C, D) non-stained sections of pancreatic tumors [23]

1.2 Hydrogels for 3D cell culture

Cells are influenced by substrate mechanics, namely, the stiffness of the substrate. Conventional culture methods rely on statically stiff 2D tissue culture plastics (TCPs). However, the ECM is a 3D structure [11, 12]. Cell behaviors in 2D environments do not necessarily recapitulate the behaviors of cells in a more natural, that is 3D, environment. Thus, researchers have shifted from cell culturing in 2D and moved towards 3D, to better understand how cells would behave in their natural environment. For example, human mesenchymal stem cells (hMSCs) were cultured on TCPs or in PEG-

gelatin hydrogels and there were distinct morphological differences between the 2D and 3D [24]. Additionally, depending on the stiffness of the PEG-gelatin hydrogels, there were morphological differences in cultured hMSCs [24].

1.2.1 Static elastic hydrogels for cell culture

Mechanically static and elastic hydrogels have been utilized to study many cell types and specific cell processes. For example, the effects of chain-growth vs. step-growth photopolymerized hydrogels was explored with hMSC culture and it was found that there was more spreading and increased viability in the step-growth polymerized networks [25]. The influence of pancreatic stromal cells on PDAC spheroids were investigated utilizing methylcellulose-based hydrogels [26]. Matrigel was utilized to fabricate organogenesis models for the study of PDAC [27]. PEG-based hydrogels were fabricated to investigate the viability of radical-sensitive MIN6 cells [28]. Additionally, the influence of β-cyclodextrin [29] and soluble tyrosine [30] on MIN6 insulin-secreting capacities were investigated in PEG-based hydrogels. When natural and synthetic scaffolds with similar storage moduli were utilized for cholangiocyte culture, they had comparable cyst formation [31]. Full-thickness skin layers were synthesized via fibroblast encapsulation and keratinocyte seeding on pectin-peptide hydrogels [32]. Electrospun methacrylate-HA (Me-HA) hydrogels were exploited to culture meniscal fibrochondrocytes and stiffer Me-HA networks promoted greater collagen-I deposition and migration into meniscal tissue, in vivo [33]. Gelatin-HA hydrogels enabled endothelial progenitor cells to synthesize complex vascular networks [34].

1.2.2 Viscoelastic hydrogels for cell culture

Viscoelastic hydrogels have also been utilized to study a wide range of cell behaviors. Naturally, the ECM is viscoelastic [16], so there has been increasing attention in hydrogels with stress-relaxing capabilities. Low molecular weight (MW) polyacrylamide (PAA) was covalently crosslinked and contained entrapped high MW

PAA, creating dissipative (i.e. stress-relaxing) hydrogels for 3T3 cell culture [35]. It was shown that 3T3 cells cultured in hydrogels that were stiffer and/or had greater stress-relaxation exhibited higher densities of paxillin patches, when compared to 3T3 cells in softer and/or less stress-relaxing hydrogels [35]. Hydrogels were formed for 3T3 cell culture with varied levels of stiffness and viscoelasticity via manipulating the MW of alginate and concentration of PEG-spacers [16]. Spreading and proliferation of encapsulated 3T3 cells increased as a function of the concentration of RGD and viscoelasticity [16]. PEG hydrogels with permanent strain-promoted azide-alkyne cycloaddition crosslinks and physical dibenzocyclooctyne-dibenzocyclooctyne crosslinks, which introduced viscoelasticity, were utilized to culture chondrocytes and it was found that stiffer and more viscoelastic hydrogels promoted proliferation and chondrogenic ECM deposition [36]. PEG hydrogels formed with reversible boronate bonds created a viscoelastic environment in which hMSCs were cultured [37]. It was found that cell-ECM interactions increased as the rate of relaxation increased [37]. Interpenetrating networks formed with reconstituted basement membrane proteins and alginate were utilized to culture MDA-231 cells and there was an increase in matrix maneuvering throughout higher plasticity interpenetrating networks [38].

1.2.3 Mechanically dynamic hydrogels for cell culture

Although there have been great efforts in understanding cellular behaviors in static 3D environments, the behavior of cells in static environments does not recapitulate the natural ECM, as it is constantly undergoing changes [11, 12]. One key aspect of the dynamic nature of the ECM lies within the increase (or decrease) in stiffness due to deposition or degradation of ECM-proteins, like collagen-I [11]. In lieu of this, mechanically dynamic hydrogel systems are increasingly in demand for greater mimetics, leading to heightened understanding of how cells truly behave in their natural environment.

For example, valvular interstitial cells (VICs) were cultured in initially soft PEG-peptide hydrogels and some were dynamically stiffened after 3-days to separate the effects of morphology and modulus [14]. In soft hydrogels, VICs exhibited greater levels of αSMA stress fibers and associated mRNA, which is characteristic of myofibroblasts [14]. In stiffened hydrogels, VICs were deactivated to a quiescent fibroblast phenotype, which suggests that VIC phenotype is directed by matrix stiffness and is independent of morphology [14].

In another example, cardiac fibroblasts were cultured in statically soft or stiff hydrogels, as well as dynamically stiffened hydrogels, which mimicked the stiffness of a healthy or fibrotic heart (i.e. soft or stiff, respectively) [39]. When cardiac fibroblasts were cultured in static hydrogels, nuclear factor of activated T-cells was localized in the cytoplasm, whereas when they were cultured on dynamically stiffened hydrogels, nuclear factor of activated T-cells was localized in the nucleus within 6-hours [39]. These findings indicate that dynamic mechanical property changes can initiate mechanotransduction pathways that would otherwise be missing in static environments [39]. In a separate study, mammary epithelial cells were cultured in Me-HA hydrogels that were dynamically stiffened to mimic the gradual matrix stiffening that occurs during breast cancer progression; the soft and stiffened hydrogels mimicked healthy and diseased tissue, respectively [40]. In both conditions mammary epithelial cells formed spheroids, but in the stiffened condition they lost epithelial characteristics and adopted mesenchymal morphologies [40]. Stiffness-mediated signaling appeared to be modulated via Twist1, TGF-β and YAP activation; culture-time prior to stiffening, as well as the degree of stiffening, affected the rate of change [40]. In another study, MCF10A (non-malignant mammary epithelial cells) were cultured in alginate hydrogels for 14-days and allowed to form acini prior to dynamic stiffening [41]. As a result of stiffening, these cells invaded from and proliferated in the mammary acini, correlating well with the knowledge that MCF10A cells cultured in stiffened environments lose epithelial characteristics and become invasive [41]. The cells maintained cell-cell contacts while migrating away from the acini, while P13K and Rac1 inhi-

bition via small molecules effectively reduced the quantity and size of invasive acini post-stiffening [41].

In addition to light or charge-based reactions, enzymatic reactions were utilized to fabricate PEG-peptide hydrogels, which were used to encapsulate COLO357 cells in an initially soft environment [42]. Dynamic stiffening was accomplished via mushroom tyrosinase (MT) [42]. A stiffened environment led to significantly smaller COLO357 spheroids, suggesting that spheroid size reductions are caused by dynamically stiffened environments [42]. In a separate study, reversibly soft/stiff PEG-peptide hydrogels were utilized to encapsulate COLO357 or hMSCs [43]. Spreading and growth of hMSCs were increased in softened hydrogels, when compared to stiffened hydrogels [43]. In stiff and stiffened hydrogels, COLO357 exhibited drug resistance, while these characteristics were not present in statically soft and less present in the softened hydrogels [43]. Dynamic PEG-peptide hydrogels were utilized to encapsulate PSCs to investigate the effects of matrix stiffening on PSC activation, namely, into myofibroblastic phenotypes [44]. MT-mediated stiffening resulted in increased expression of αSMA and HIF-1α, suggesting activation into myofibroblastic phenotype [44].

1.2.4 Prior examples of biomimetic hydrogels for cell culture

Biomimetic hydrogels can be generally defined as systems that contain tunable matrix mechanics and permeability, integrin-binding ligands, and matrix degradability [45], although not all contain each of these properties. These hydrogels can be formed taking advantage of various crosslinking methods such as: chain-growth, step-growth, or mixed-mode photopolymerization, as well as enzymatic reactions and supramolecular interactions [45]. The purpose of biomimetic hydrogels is to enable the study of how cells interact with their environment and with other cells, in systems that are emulative of their natural niches.

All biomimetic hydrogels should contain integrin-ligands and matrix metalloproteinase (MMP)-degradable sites. For example, PEG-peptide hydrogels were utilized

to culture hMSCs and MIN6 [28] or MIN6 cells alone [30]. RGD-tagging was exploited to promote cell attachment in otherwise bio-inert systems [30] and in Me-HA hydrogels utilized to culture meniscal fibrochondrocytes [33]. Other PEG-based hydrogels were dynamically stiffened and included laminin-111 [46], HA, [47], or mechanical matching of hydrogels to healthy and diseased tissue [39].

1.3 Gelation mechanisms

Hydrogels are attractive cell-culture platforms due to their wide range of reaction modes and chemistries of gelation. Commonly used crosslinking methods include, but are not limited to, chain-growth, step-growth, and mixed-mode photopolymerization, enzyme-mediated or click-chemistry-mediated polymerization, and supramolecular assembly [45]. Additionally, hydrogel crosslinking can be initiated with light (either UV or visible), or induced by temperature changes, ionic interactions, or enzymatic reactions. With a plethora of gelation modes and chemistries, hydrogels are easily tuned to fit specific needs, such as elastic, storage and/or loss moduli, tethering of bioactive molecules, and degradability. Advantages of hydrazone bonds (a click-chemistry between aldehyde and hydrazide moieties) lies within their ability to impart more viscoelasticity into the system and the lack of necessity for an initiator [34, 48]. A disadvantage is the lack of spatiotemporal crosslinking control [45].

1.3.1 Thiol-norbornene gelation for cell culture

Thiol-norbornene crosslinking, shown in Figure 1.3, has been widely utilized for biomimetic hydrogels due to its fast reaction rates, cytocompatibility, spatiotemporal control of crosslinking kinetics, and facile tethering of bioactive molecules [49]. Conventionally, thiol-norbornene gelation is initiated by UV light (wavelength = 365 nm) irradiation. Alternatively, Eosin-Y can be used as the sole-photoinitiator for visible light initiated gelation (400 – 700 nm) [28, 30, 49, 50]. With long-wave UV-light and a photo-initiator (such as lithium phenyl-2,4,6-trimethylbenzoylphosphinate or

LAP), primary networks of crosslinked thiol-norbornene hydrogels were utilized for cell-culture [14, 25, 32, 51–53]. Another utilization of the thiol-norbornene photo-click reaction is immobilization of biomimetic peptides that enable cell-attachment and/or MMP-degradation [42].

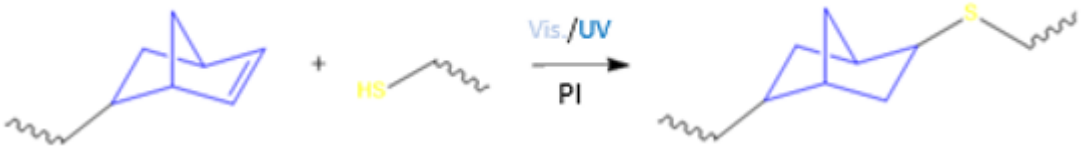

Fig. 1.3. Photo-click thiol-norbornene crosslinking

1.3.2 Tetrazine-olefin click chemistry

The inverse electron Diels-Alder addition (iEDDA) click-chemistry takes place between 1,2,4,5-tetrazines (Tz) and olefins (e.g., norbornene or NB) [54]. Due to iEDDA biorthogonality (i.e. biological activity of biologics, such as DNA and enzymes, undisturbed), high-reaction speed, and hydrolytic stability [54] these reactions are becoming increasingly popular. Tz ligation with trans-cyclooctyne (TCO) permitted temporal control of hydrogel stiffness and biomarker presentation for encapsulated hMSCs [47]. A hydrophilic polymer with unreacted Tz formed a primary network with thiolated HA HA-SH, after which the network could be stiffened via TCO-modified HA (HA-TCO) or cell-attachment could be increased via TCO-modified RGD (RGD-TCO) [47]. In another 3D study, PEG-gelatin hydrogels formed via click Tz-NB reactions encapsulated hMSCs [21]. As the stiffness of hydrogels increased, the amount of hMSC spreading decreased [21]. The Tz-NB reaction schematic can be seen in Figure 1.4.

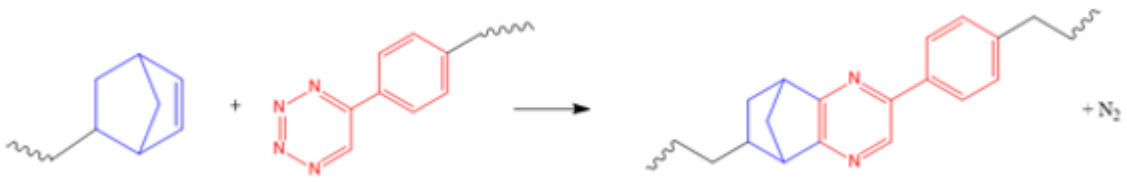

Fig. 1.4. Click tetrazine-norbornene crosslinking

1.3.3 Hydrazone hydrogels

Hydrazone crosslinked hydrogels are injectable, self-healing, and stimuli responsive (e.g., pH or redox triggers) [34, 55]. The hydrazone reaction schematic can be seen in Figure 1.5. They have been predominantly used to investigate the effects of stress-relaxation on cells in culture. For example, RGD-modified alginate substrates were utilized for culturing mouse myoblasts in 2D [56]. In this study, covalent hydrazone crosslinks were formed with oxidized alginate and adipic acid dihydrazide, and ionic crosslinks were formed with divalent calcium ions and alginate [56]. By manipulating the density of covalent or ionic crosslinks, this group was able to create hydrogels with varied elastic and viscoelastic (i.e. stress-relaxation) profiles, respectively [56]. In another example, A549 cells encapsulated in oxidized alginate and propionohydrazide-modified PEG hydrogels were viable after 24-hours [48]. In another 3D study, gelatin- and oxidized dextran-based hydrogels loaded with endothelial colony-forming cells were subcutaneously injected into backs of mice [34]. The encapsulated and injected endothelial colony-forming cells were able to form complex vascular networks in vivo [34].

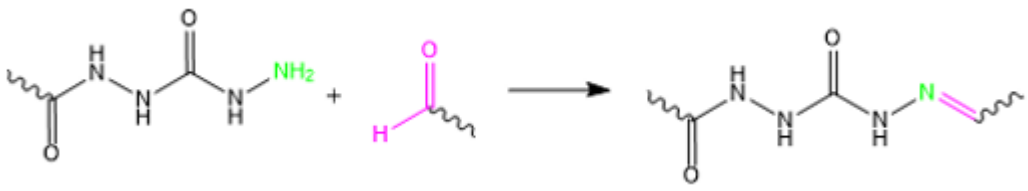

Fig. 1.5. Click aldehyde-hydrazide hydrazone crosslinking

1.4 Rationale for the thesis

To recapitulate the natural progression of healthy to diseased pancreatic tissue (i.e. HA presence and increase in matrix stiffness), prior studies have utilized gelatin-HA hybrid hydrogels that can be dynamically stiffened to culture PDAC cells [51,52]. In these examples, however, HA was a part of the primary hydrogel network and only matrix stiffness was dynamically altered via enzymatic reactions [51, 52]. As previously stated, in the natural PDAC progression, there is an increase in matrix stiffness and an accumulation of secreted HA [17, 18]. In an effort to improve the design of a dynamic hydrogel system that recapitulates a stiffening matrix with accumulation of HA deposition, this work explores the use of chemically modified HA to stiffen a cell-laden hydrogel.

2. OBJECTIVES

To gain an understanding of how synergistic increase in matrix stiffness and accumulation of HA affect PDAC cells in 3D culture, soft PEG-gelatin hydrogel networks were formed, followed by dynamic stiffening with chemically modified HA. The primary PEG-gelatin hydrogels were crosslinked by either thiol-norbornene or aldehyde-hydrazide click-chemistry, whereas stiffening was accomplished by chemically modified HA via tetrazine-norbornene or aldehyde-hydrazide click-chemistry. After establishing a dynamic hydrogel platform, initially formed with thiol-norbornene crosslinks and stiffened by hydrazone crosslinks, the system was exploited for PDAC cell culture, in which the viability and metabolic activity where characterized via live/dead staining and alamarblue, respectively, and encapsulated cells were treated with chemotherapeutics. This system was developed to gain understanding into the synergistic effects of matrix stiffening and increased presence of HA on PDAC cells. To achieve these goals, the following objectives were proposed:

- To integrate orthogonal click-chemistries for forming PEG-gelatin hydrogel systems with independently tunable mechanical and biological properties.

  Specifically, hydrogels were crosslinked via thiol-norbornene, tetrazine-norbornene, or aldehyde-hydrazide click-chemistries. In one network, norbornene was in excess, relative to thiol, for tetrazine-based stiffening. In another network, hydrazide was in excess, relative to aldehyde, for aldehyde-based stiffening.

- To utilize tunable PEG-gelatin hydrogel system for encapsulation of PDAC cells to study the synergistic effect of stiffening and accumulating-HA on PDAC cell fate.

Specifically, cell viability, spheroid size, and morphology of encapsulated PDAC cells in stiffened and HA-accumulating matrices were monitored via live/dead stained cell images. Additionally, relative metabolic activities of PDAC cells, before and after stiffening, were assessed via alamarblue reagent. Chemotherapeutic efficacy of gemcitabine (GEM) was also explored in response to the stiffened and HA-accumulating matrices.

3. MATERIALS AND METHODS

3.1 General Materials

Type B gelatin (bloom 225) was purchased from Electron Microscopy Sciences. Carbic anhydride (CA), carbohydrazide (CDH), and 1-ethyl-3-(3-dimethylamino propyl)carbodiimide HCl (EDC) were purchased from Acros Organics. Sodium hyaluronate (14.8 and 74 kDa) were purchased from Lifecore Biomedical. Heparin sodium salt was purchased from Celsus Laboratories. Tetrazine-amine (Tz-amine) was purchased from Click Chemistry Tools. N-hydroxysuccinimide (NHS) and N,N-diisopropylethylamine (DIEA) were purchased from Tokyo Chemical Industries. Hydroxy benzotriazole (HOBt) was purchased from Oakwood Chemical. Alamar blue and 3-(4,5-dimethylthiazol-2-yl)-2,5-diphenyltetrazolium bromide (MTT) were purchased from Fisher. Poly(ethylene glycol)-tetra-propionaldehyde (PEG4pAld) and poly(ethylene glycol)-tetra-thiol (PEG4SH), shown in Figure 3.1,were purchased from Layson Bio. Viability (live/dead) kit was purchased from Biotium. Rabbit anti-CD44 antibody and goat anti-rabbit IgG-TR were purchased from Ray Biotech and Santa Cruz Biotech, respectively. N2 and N21 MAX media were purchased from R and D Systems. High glucose DMEM and DMEM/ham's F-12 50/50 were purchased from GE Healthcare and Corning, respectively. DPBS, fetal bovine serum (FBS) and 100 antibioticantimycotic were purchased from Corning. 1,9-dimethyl-methylene blue (DMMB) zinc chloride and all other chemicals were purchased from Sigma-Aldrich, unless otherwise noted.

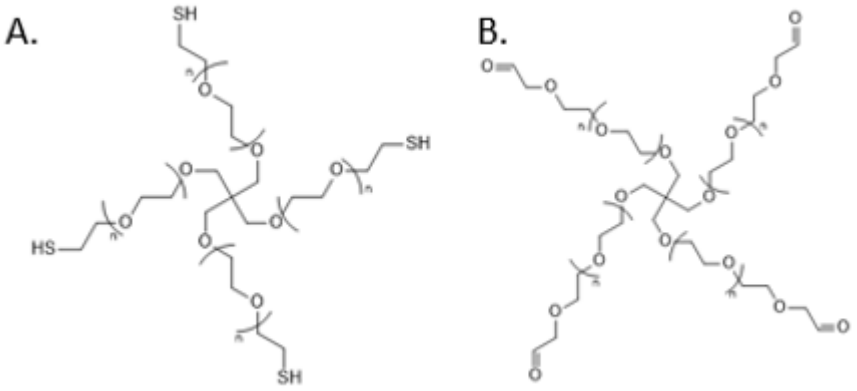

Fig. 3.1. Structure of PEG4SH (A) and PEG4pAld (B)

3.2 Macromer Synthesis and Characterization

8-arm poly(ethylene glycol) (PEG8NB) was synthesized and characterized following published procedures [42, 57]. Gel(B)NB was synthesized following a published procedure [25]. Gel(B)NB substitutions were characterized via Fluoraldehyde assay using unmodified gelatin with known concentrations as a standard. In Figure 3.2, a synthesis schematic of Gel(B)NB is shown.

Gel(B)NB-CDH was synthesized with the following procedure. First, Gel(B)NB was dissolved in 50 mL PBS, which was kept warm and stirred via rotovap. Gelatin solution was then moved to 45^{o}C oil bath and CDH was added to the solution and mixed until dissolved. EDC and HOBt were dissolved in 13 mL DI-H2O and amine-free dimethylformamide (DMF) (1:1 v/v). Once dissolved, the EDC and HOBt mixture was added to the gelatin solution. Subsequently, the pH was adjusted to 5 and the reaction was allowed to occur for 24-hours at 45^{o}C. After the 24-hours, the solution was transferred to a dialysis membrane of 12-14 kDa molecular weight cut-off (MWCO), where it underwent dialysis for 3-days at 40^{o}C (first day 0.1 M NaCl added and 2^{nd} and 3^{rd} day drops of HCl were added). After dialysis, the solution was frozen and lyophilized. Functionalization of CDH was characterized via 2,4,6-trinitobenzene

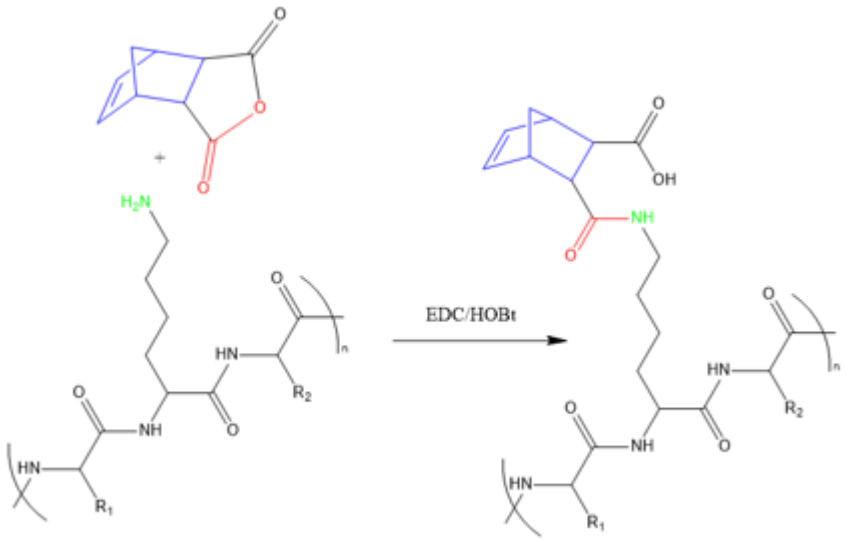

Fig. 3.2. Synthesis schematic of Gel(B)NB

sulfonic acid (TNBSA) assay, comparing Gel(B)NB-CDH to a standard curve created from ADH. In Figure 3.3, a synthesis schematic of Gel(B)CDH is shown.

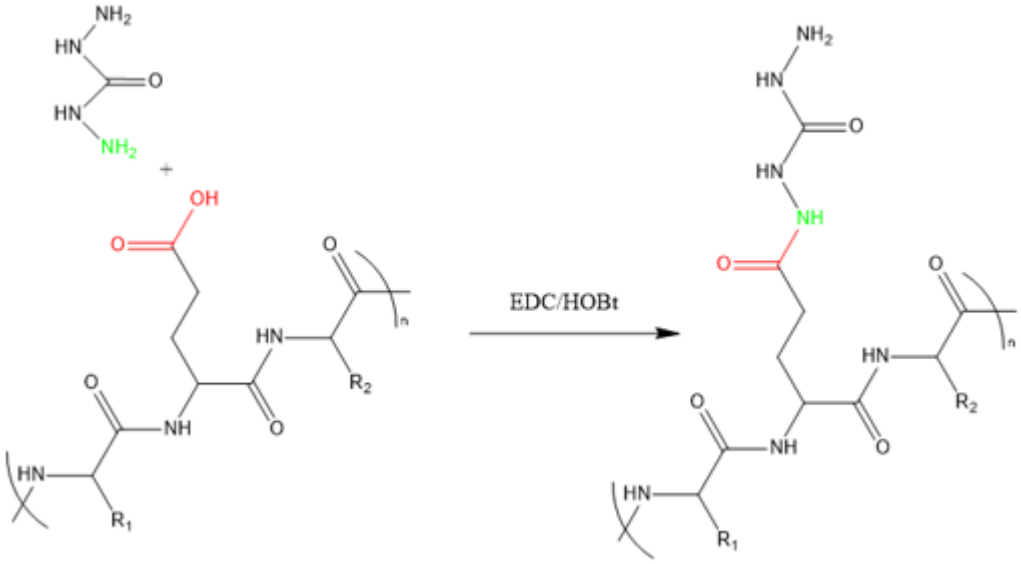

Fig. 3.3. Synthesis schematic of Gel(B)CDH

Heparin-tetrazine (Hep-Tz) was synthesized by dissolving, at room temperature with stirring, heparin sodium salt (16.3 kDa) in 15 mL ddH_2O. Subsequently, 5-fold excess EDC and NHS were dissolved in the heparin solution. Prior to Tz-amine HCl salt addition, there was a 30-minute activation of carboxylic acids via EDC/NHS. Separately, 5-fold excess Tz-amine HCl salt was dissolved at room temperature, with stirring and protection from light, in 5 mL ddH_2O. Once dissolved, the heparin and Tz-amine solutions were combined stirred in the dark for 16-hours. Dialysis in ddH_2O, with a 3500 MWCO cellulose membrane, was performed at room temperature in the dark for 2-days. After dialysis, the product was frozen and lyophilized, while being protected from light. HA-tetrazine (HA-Tz; 14.8 or 74 kDa) was synthesized in a similar manner, adjusting the concentrations of EDC, NHS and Tz-amine HCl salt to carboxylic acids available in HA compared to heparin. To quantify the conjugation of Tz-amine to heparin, a Synergy HT microplate reader at 523 nm was used to create a standard curve of Tz-amine HCl salt and compared to Hep-Tz or HA-Tz solution.

Four-arm PEG-tetrazine (PEG4Tz) was synthesized by first dissolved PEG4ASA (10 kDa) in 2 mL amine-free DMF. Subsequently, HATU was added to the solution and stirred for 10-minutes at room temperature. Simultaneously, Tz-amine HCl salt was dissolved in 500 μL amine-free DMF and stirred for 20-minutes. After the 10- and 20-minutes were complete, the two solutions were mixed together and 5-fold excess DIEA was added to the reaction vessel. The final solution is stirred and protected from light for 16-hours. After 16-hours, the solution is transferred to a 3500 MWCO dialysis membrane and dialyzed for 2-days, still protecting from light. Following dialysis, the product was frozen and lyophilized prior to quantification of Tz substitution. PEG4Tz was similarly quantified to Tz conjugation in HA-Tz and Hep-Tz.

For oxidized-dextran (oDex) synthesis, first NaIO4 was dissolved in 200 mL ddH2O and the solution was protected from light. The amount of NaIO4 dissolved varied depending on the desired degree of oxidation. Dextran (100 kDa) was then dissolved into the NaIO4 solution and left stirring overnight while protected from light. The

next morning, the solution was transferred to a 12-14 kDa MWCO dialysis membrane and dialyzed for 3-days. After dialysis, the solution was frozen and lyophilized to collect product. Theoretical functionalization was ascertained via concentration of diols that could be ring-opening oxidized. For oxidized-HA (oHA; 14.8, 74, or 740 kDa) synthesis, the procedure was the same as oDex. The concentration of carboxylic acids per weight percent did not change with molecular weight, thus, the amount of $NaIO_4$ used for varied degrees of oxidation was kept constant for different MW oHA synthesis.

Tetrazine modified macromers (TMMs) are shown in Figure 3.4 and oxidized molecules are shown in Figure 3.5.

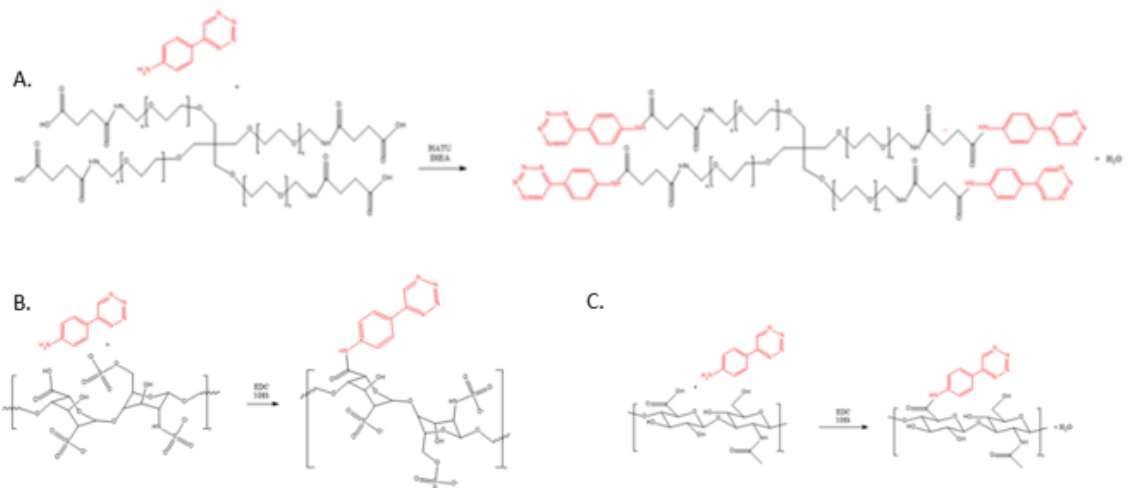

Fig. 3.4. Synthesis schematics for PEG4Tz (A), Hep-Tz (B) and HA-Tz (C)

3.3 Hydrogel Fabrication and Characterization

Hydrogels were initially crosslinked with two different methods: (1) photo-click thiol-norbornene (both UV and visible light) and (2) hydrazone. For hydrogels formed via UV-light, gel precursors were prepared with desired concentrations of LAP, NB- and SH-containing macromers and mixed well via vortexing. Subsequently, pre-mixed

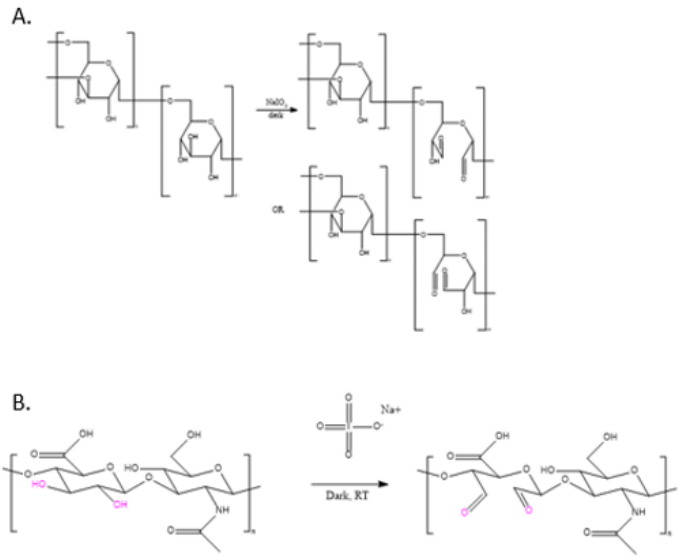

Fig. 3.5. Synthesis schematics for oDex (A) and oHA (B)

precursor solution was pipetted between two glass slides, separated by 1 mm thick spacers, and exposed to 5 mW/cm^2 365 nm light for 2-minutes via Blak-Ray XX-15M UV Bench Lamp.

For hydrogels formed via visible light, gel precursors were prepared in a similar manner to that described above. Subsequently, pre-mixed precursor solution was pipetted between two glass slides, separated by 1 mm thick spacers, and exposed to 70 kLux visible light for 5-minutes via AmScope Cold-Light Source Haloid Lamp.

Hydrogels formed via spontaneous hydrazone crosslinks were prepared by initially creating two precursor solutions that would leave excess CDH (and NB) in the hydrogel: (1) Gel(B)NB-CDH and PBS and (2) oHA. Molds were then placed on glass slides and the negative space was coated with plasma oxygen. Due to the small volume of (2) used in each gel, (2) was pipetted into the negative space within the mold followed by (1). Gelation begun upon contact, so there was very little working time. In efforts to homogenize the mixture, gentle swirling of the pipette tip was employed starting from the outside and working in. Binder clips were then placed on each end of the glass slide with a mold and the entity was inverted and placed within a hu-

midifying chamber with a damp piece of cloth to ensure hydration. These gels were given 30-minutes to form completely.

Each hydrogel was prepared with ideal dimensions of 1 mm thickness and 8 mm diameter. After fabrication, each hydrogel was given at least 1-hour to swell to equilibrium in DPBS + 1% P/S, prior to rheological characterization. Generally, stiffening was initiated immediately following pre-stiffened rheological characterization and lasted for 24-hours. In a few cases, stiffening endured for longer than 24-hours.

Quantification of G' and G" (shear/storage and loss modulus, respectively) for fabricated hydrogels was accomplished via parallel plate, strain sweep rheometry on Bohlin CVO 100 Digital Rheometer. Strain ranged from 0.1-5%, at an oscillating frequency of 1 Hz, over the course of 100 seconds and testing was conducted at room temperature. The first few data points were removed from analysis to allow the stabilization of the rheometer and the values were averaged to obtain G' and G".

3.4 Cytotoxicity and Alamarblue assays

Cytotoxicity studies for HA-Tz and oHA were conducted in 2D. PANC-1 were plated in a 96-well plate at 50,000 cells/mL and allowed to attach and grow for 2-3 days. Subsequently, varied concentrations of soluble, chemically-modified HA were added to wells in quadruplicate. Soluble HA was kept in solution for 24-hours. Subsequently, media + MTT reagent was added to each well for a specified amount of time before the media + MTT reagent was carefully aspirated. Metabolic product was solubilized in dimethyl sulfoxide (DMSO) and mixed well (via pipette) before transfer to a separate well plate for absorbance reading at 590 nm via Synergy HT microplate reader. DMSO was used as a blank.

Alamarblue was conducted in 3D for encapsulated cells. For this procedure, all solutions and materials were protected from light. First, a solution (i.e. alamarblue solution) of 1-part alamarblue reagent and 9-parts high glucose DMEM media (+10% FBS and 1% P/S) was created. Second, encapsulated cells were transferred to new

wells prior to addition of alamarblue solution. The encapsulated cells were maintained in alamarblue solution for a number of hours (varied depending on cell type and density). Subsequently, encapsulated cells were transferred to new wells and refreshed with new media. The alamarblue solution was then carefully mixed, in each well, and a portion was transferred to a new well plate for fluorescence readings at excitation and emission wavelengths of 560 and 590 nm, respectively, via Synergy HT microplate reader. Pure alamarblue was used as a blank. Fluorescence values were normalized to non-treated encapsulated cells.

3.5 Cell maintenance and encapsulation

PANC-1 cells were cultured on TCPs in high glucose DMEM with 10% FBS and 1% P/S added for additional growth factors and sterility, respectively. Media was refreshed every 2-3 days, according to the need. The cells were allowed to grow until they reached confluence of around 70% prior to passaging and/or encapsulating.

For encapsulations, all hydrogel and post-modification materials were sterile-filtered through 22 μm filters. Additionally, some materials, namely modified gelatin and HA, were further sterilized with germicidal, mid-wave UV (i.e. 254 nm).

Encapsulating PANC-1 in visible-light crosslinked hydrogels was accomplished in syringes with their tops cut off. The volume of each hydrogel was 25 μL and the encapsulation density was 1,000,000 cells/mL. If there were greater than 10% dead cells after trypsinizing, encapsulation was postponed. The gelation parameters were consistent with hydrogel fabrication for rheological characterization (i.e. 70 kLux for 5-minutes via AmScope Cold-Light Source Haloid Lamp).

Encapsulating PANC-1 in UV crosslinked hydrogels was also accomplished in syringes with their tops cut off. The volume of the hydrogels and encapsulation densities were maintained between UV- and visible-light hydrogels. Again, if there were greater than 10% dead cells after trypsinizing, encapsulation was postponed. The gelation

parameters were consistent with hydrogel fabrication for rheological characterization (i.e. 5 mW/cm^2 for 2-minutes via Blak-Ray XX-15M UV Bench Lamp).

Similar to culturing on TCPs, media was refreshed every 2-3 days, as needed. Stiffening was generally accomplished overnight from Day 1 to Day 2 (e.g. encapsulation was on Day 0). In some cases, stiffening was delayed until Day 7, to allow clustering of cells to occur.

3.6 Spheroid media preparation

Spheroid media was prepared following the procedure in [58]. Briefly, 20 ng/mL endothelial growth factor (EGF) and fibroblast growth factor (FGF) were added to 100 mL high glucose DMEM:F12 with 1% P/S . Additionally, 2% N21-MAX and 1% N2-MAX media supplements were added to the media.

3.7 Live/dead staining and imaging

To characterize the viability and morphology of encapsulated cells, live/dead staining was utilized. Calcein AM and Ethidium III was used for live and dead staining, respectively. Hydrogels with encapsulated cells were transferred to new well plates and washed 3x with DPBS for 5-minutes prior to the addition of staining solution. Once staining solution was added, the gels were protected from light and incubated for 1-hour on a stirring plate to allow the stain to diffuse. Subsequently, excess stain was removed from the gels with another series of 3 5-minute washes with DPBS. Hydrogels were then transferred onto glass slides for imaging. Images were acquired via LionHeart FX automated microscope and image analysis was conducted in ImageJ.

3.8 Drug responsiveness in encapsulated cells

To characterize drug resistance of encapsulated cells, gemcitabine was used. A previously reported lethal dose, 50% (LD50) concentration of 1 μM gemcitabine was

employed for drug studies [59], as well as 4 μM and 10 μM to see an increased cell death profile. Cells were allowed to grow in hydrogels prior to stiffening, after which gemcitabine was added to each well. Gemcitabine and media were refreshed daily until the end of drug treatment, which lasted 4-days. To quantify metabolic activity and viability, AB and live/dead staining was utilized, respectively. Morphology was also monitored via live/dead staining. Imaging was conducted with LionHeart and image analysis was conducted in ImageJ.

3.9 Immunofluorescence

To visualize CD44 expression on encapsulated cells, immunofluorescence was utilized. Immediately following drug treatment, hydrogels were washed (2x) and cells were fixed with 4% paraformaldehyde. Hydrogels were washed again (3x) and cells were blocked and permeabilized with bovine serum albumin (BSA) and Triton-X-100 solution overnight at 4^oC. The next day, BSA and Triton-X-100 solution was replaced with primary antibody (i.e. rabbit anti-CD44), BSA, and Triton-X-100 solution and stored at 4^oC overnight. Hydrogels were then washed (3x) with BSA and Triton-X-100 solution and stored at 4^oC in secondary antibody (goat anti-rabbit-TR), BSA, and Triton-X solution overnight, while being protected from light. Protecting hydrogels from light, they were washed (3x) and stained with 4',6-diamidino-2-phenylindole (DAPI). Following DAPI staining, hydrogels were washed again (3x) while being protected from light and subsequently imaged.

3.10 Statistical analysis

GraphPad Prism was the data analysis tool employed for all studies. Hydrogels were prepared in triplicate for mechanical testing. Cell studies were repeated at least once for verification of results. All statistical analysis was conducted using one-way ANOVA with a Bonferroni post-test analysis. In summary, * represents $p < 0.05$, ** represents $p < 0.001$, and *** represents $p < 0.0001$.

4. RESULTS AND DISCUSSION

4.1 Tunable visible-light crosslinking of thiol-norbornene hydrogels

One of the goals of this study was to create a tunable visible-light initiated thiol-norbornene primary hydrogel network to mimic the stiffness of healthy pancreatic tissue. It is known that many factors, such as exposure time to light and concentration of photo-initiator would influence the crosslinking densities of hydrogels. Thus, as seen in Figure 4.1, the initial storage modulus of gelatin-based hydrogels was readily tuned via modulation of visible light exposure time and the concentration of photoinitiator (i.e. LAP) within the gel precursor solution.

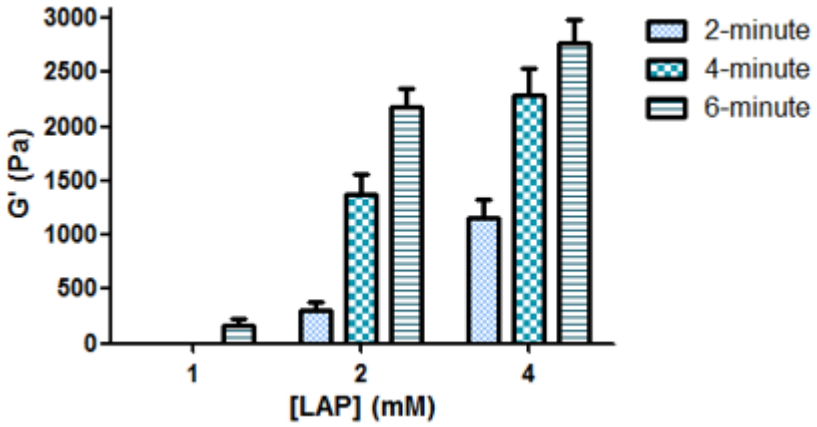

Fig. 4.1. **Effect of photoinitiator concentration and polymerization time on visible light initiated crosslinking of Gel(B)NB (5 wt%) hydrogels.** PEG4SH: 1 wt% (R=0.45); Visible light intensity: 70 kLux

Every hydrogel formed contained the same macromer content (Figure 4.1). The initial storage modulus, and crosslinking density, was tuned as a function of exposure time and LAP concentration (i.e. more exposure time or LAP resulted in an increased

initial storage modulus). When using 1 mM LAP in the gel precursor, only the highest exposure time formed a gel and it was soft (i.e. 170 Pa) and difficult to handle. When using 2 mM LAP, gels formed under all exposure times. The lowest storage modulus was 300 Pa and the highest was 2,200 Pa, for 2- and 6-minute exposure time, respectively. When using 4 mM LAP, again, gels formed under each exposure time. The storage modulus, of gels formed with 2-minutes of exposure time, more than doubled (i.e. 1,150 Pa) when compared to those formed with 2-minutes exposure time and 2 mM LAP. The highest storage modulus, from 6-minute exposure time, had a more modest increase of 25%, which was not significant, when compared to the gels formed with 2 mM LAP. A few conditions would lead to physiologically relevant stiffness, when compared to healthy pancreatic tissue [17]. Naturally present cell-attachment and MMP-degradable sites within this gelatin-based hydrogel system make it highly attractive and biomimetic.

Another commonly used method to control the crosslinking density of hydrogel networks lies within modulation of the concentrations of crosslinker. Thus, by manipulating the R-value (i.e. [SH]:[NB]), the crosslinking densities of PEG-based hydrogels were tuned (Figure 4.2).

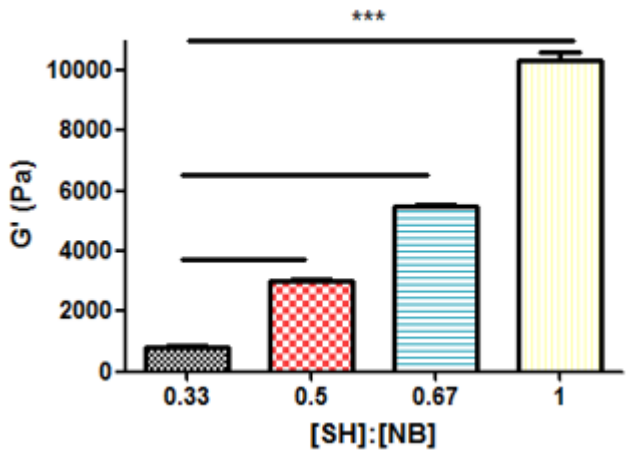

Fig. 4.2. **Controlling initial crosslinking density of PEG8NB (3 wt%) hydrogels via tuning R-value (i.e., [SH]:[NB]).** LAP: 4 mM; Visible light intensity: 70 kLux; Polymerization time: 5-minutes

Crosslinking densities, and initial storage moduli, were tuned via maintaining a constant concentration of NB-containing macromer and adjusting the concentration of thiol-containing macromer. Thus, hydrogel crosslinking density correlates positively to the R-value (between 0.33 and 1). Specifically, with 3-fold excess of NB to thiol moiety (i.e., R=0.33), gels were formed with storage moduli of less than 1,000 Pa. At a stoichiometric ratio of thiol and NB (i.e., R = 1), there was a significant increase in storage moduli, reaching above 10 kPa. The hydrogel formed with an R-value of 0.33 is physiologically relating to healthy pancreatic tissue stiffness [17] and could be considered biomimetic if it were tagged with cell-attachment and MMP-degradable sequences [45].

4.2 Tunable crosslinking of hydrazone hydrogels

In addition to thiol-NB photopolymerization, hydrazone crosslinked primary hydrogel networks can also be used to present physiologically relevant stiffness. Due to the spontaneous reactivity of this crosslinking, an initiator is not required for the gelation. Thus, manipulation of macromer content was employed in efforts to tune crosslinking density (Figure 4.3).

As shown in Figure 4.3, the storage modulus of hydrazone hydrogels increased as the content of macromer increased (i.e., Gel(B)NB-CDH and PEG4pAld). Note that in this chemistry, hydrogels were crosslinked by CDH-aldehyde reaction (Figure 1.5). Maintaining a constant molar ratio of aldehyde to CDH and adjusting the macromer content provided an efficient means to tune this systems stiffness, as indicated by significant stiffness differences between the hydrogels with various macromer content. Although this system requires no initiator, the resulting initial gel moduli were much higher than what would be considered for a healthy tissue, when compared to healthy pancreatic tissue (i.e., G’ 1000 Pa) [17].

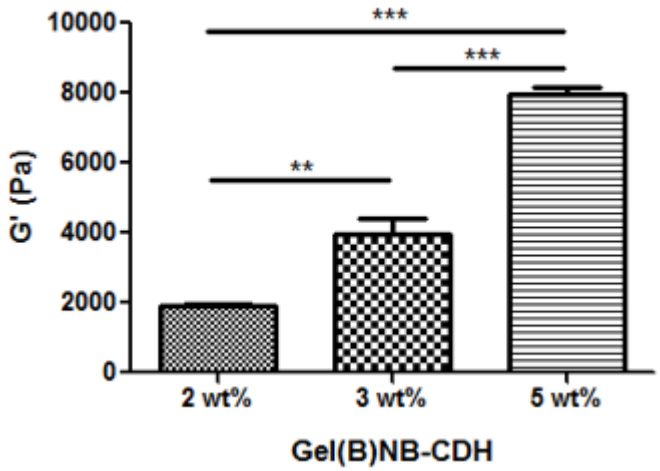

Fig. 4.3. **Controlling initial crosslinking density of Gel(B)NB-CDH hydrogels via tuning macromer concentration while maintaining Q-value (i.e., [Ald]:[CDH]).** PEG4pAld: 1.56, 2.34, and 3.9 wt%, respectively; Q=0.5

4.3 Tunable crosslinking of UV-light thiol-norbornene hydrogels

Owing to the presence of dual functional groups, Gel(B)NB-CDH can be cross linked either by hydrazone click chemistry or by thiol-NB photopolymerization. Similar to tuning crosslinking density of visible-light initiated thiol-NB hydrogels, UV-initiated gelation could be used to tune hydrogel modulus within the stiffness range of healthy pancreatic tissue. In this gelatin-based hydrogel system, a constant R-value of 0.5 (i.e. 2-fold excess NB-to-thiol) was utilized to allow for photo-click thiol-NB based biomolecule-tagging or further stiffening. Although maintaining a constant R-value was employed, the system still held potential to be tuned via concentration of LAP in the precursor. In Figure 4.4, the effects of manipulating the precursor LAP concentration is shown.

As seen in Figure 4.4, the crosslinking density of this hydrogel system increased as a function of the concentration of LAP within the gel precursor solution. Each gel formulation was identical, with the only difference being the concentration of LAP. This provides another method for tuning the crosslinking density within the UV-light

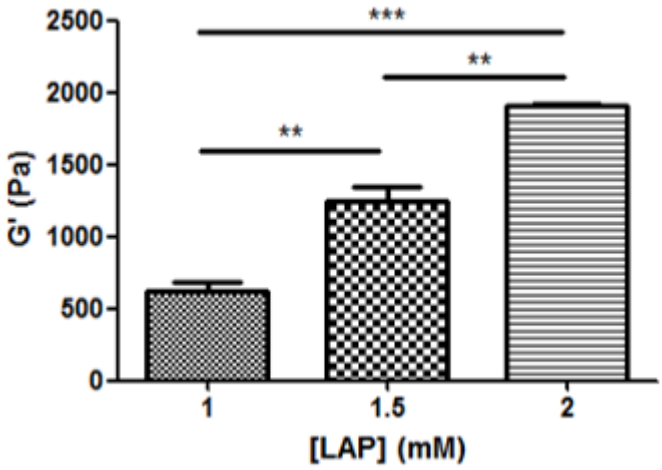

Fig. 4.4. **Effect of photoinitiator concentration on UV light initiated crosslinking of Gel(B)NB (5 wt%) hydrogels.** PEG4SH: 1 wt% (R=0.5); UV light intensity: 5 mW/cm^2; Polymerization time: 2-minutes

crosslinked thiol-norbornene primary network. The hydrogels formed with 1 and 2 mM LAP were slightly too soft and stiff, respectively, when compared to healthy pancreatic tissue [17]. However, the hydrogels formed with 1.5 mM LAP mimicked the stiffness of healthy pancreatic tissue well [17]. Due to the natural presence of cell-attachment and MMP-degradable sequences within gelatin, this is an attractive, biomimetic system.

4.4 Click Tz-NB reaction for temporally controlled stiffening of visible-light hydrogels

Hydrogels were formed with excess click reactions with Tz for temporally controlled stiffening. Utilizing one of the formulations of gelatin-based networks, stiffening with TMMs (either Hep-Tz or HA-Tz) was attempted (Figure 4.5).

Starting with the same hydrogel composition and similar storage moduli, the hydrogels in Figure 4.5 were exposed to 0.5 wt% soluble HA-Tz or Hep-Tz for 24-hours. After 24-hours of exposure, the storage moduli of the hydrogels did not change

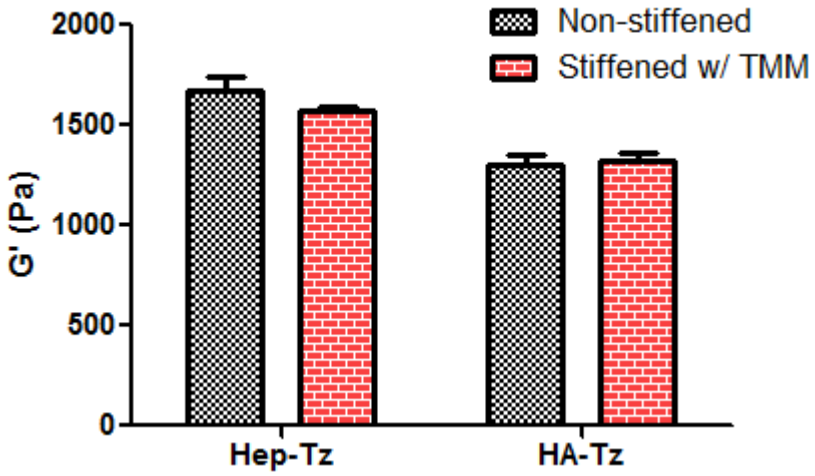

Fig. 4.5. **Effect of TMM (0.5 wt%) on stiffening of Gel(B)NB (5 wt%) hydrogels.** PEG4SH: 1.5 wt% (R=0.45); LAP: 4 mM; Visible light intensity: 70 kLux; Polymerization time: 5-minutes

significantly, suggesting that additional crosslinks did not occur. After some consideration, it was thought that a potential issue could be that the NB groups were on gelatin. Gelatin is a natural material that is charged and an irregularly structured. The charged and irregularly structured nature of this material might inhibit Tz-NB crosslinking. Thus, the same method of stiffening was explored with a PEG-based hydrogel (Figure 4.6).

Unlike in gelatin-based networks, TMM stiffening was more effective in PEG-based networks. This indicated that there is an issue causing hinderance of the click Tz-NB reaction when NB is on gelatin (cause unknown), but not PEG. This being said, PEG-based systems were further explored in efforts to tune the stiffening capacity provided from TMMs. In Figure 4.7, the effect of R-value on the resulting stiffness increases was explored.

As indicated with gelatin-based thiol-norbornene hydrogels, the initial storage modulus (i.e. crosslinking density) could be tuned as a function of R-value. Physically, this means that as the R-value increases, so does the number of crosslinks, up to a theoretical 100% maximum achieved with an R-value of 1. Thus, it was expected

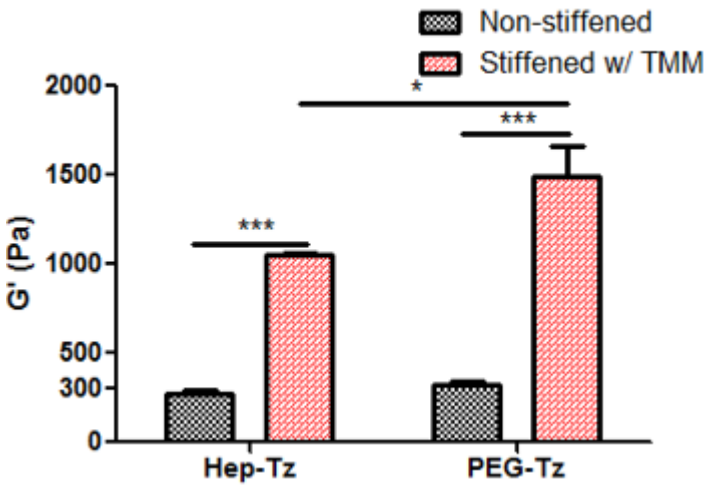

Fig. 4.6. **Effect of TMM (0.5 wt%) on crosslinking of PEG8NB (3 wt%) hydrogels.** DTT: 1.62 mM (R=0.45); LAP: 4 mM; Visible light intensity: 70 kLux; Polymerization time: 5-minutes

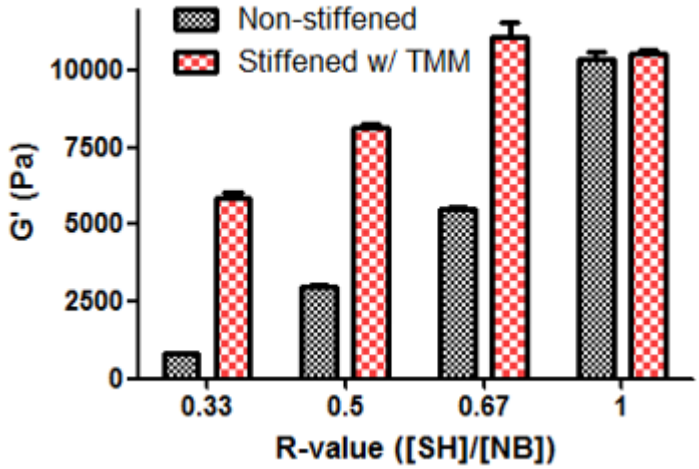

Fig. 4.7. **Controlling HA-Tz (0.5 wt%) stiffening of PEG8NB (3 wt%) hydrogels via R-value manipulation.** PEG4SH: 0.8, 1.2, 1.6, or 2.4 wt%, respectively; LAP: 4 mM; Visible light intensity: 70 kLux; Polymerization time: 5-minutes

that as the R-value increased, the stiffening effect (i.e. fold-increase in stiffness) would decrease. As shown in Figure 4.7, this is exactly what was shown. There was

a greater than 6-fold to 0-fold increase in stiffness as a result of 24-hour 0.5 wt% HA-Tz stiffening, for R=0.33 and R=1, respectively. Interestingly, the maximum stiffness achieved was in the R=0.67 case, which was slightly higher than the stiffness of the non-stiffened or stiffened R=1 hydrogels. This suggests that Tz-NB crosslinks provide a more rigid backbone than SH-NB crosslinks, likely due to the bulky Tz structure, but this idea was not further explored.

Other methods for tuning the stiffening effects of this system, while maintaining a constant macromer content, photo-initiator content, and R-value, included: (1) manipulating the concentration of soluble TMM for stiffening and (2) manipulating the substitution of Tz within the TMMs, while utilizing the same concentration of TMM for stiffening. The results of (1) and (2) can be seen in Figures 4.8 and 4.9, respectively.

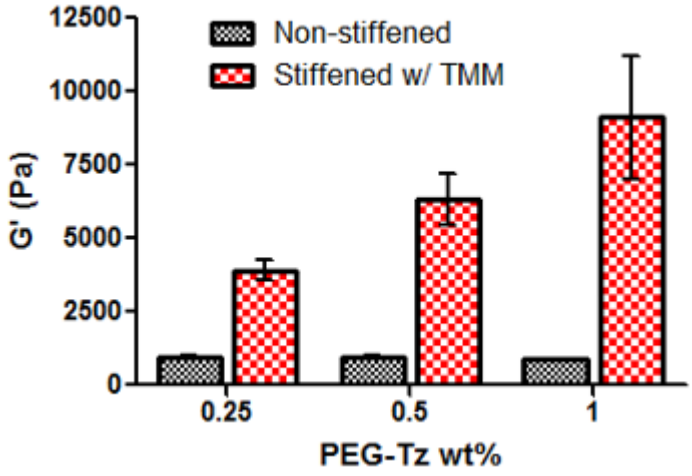

Fig. 4.8. **Tuning stiffening of PEG8NB (3 wt%) hydrogels via manipulating PEG4Tz concentration.** PEG4SH: 1.2 wt% (R=0.5); LAP: 4 mM; Visible light intensity: 70 kLux; Polymerization time: 5-minutes

Starting with the same macromer and photo-initiator content, as well as R-value, yielded hydrogels that had similar moduli after initial crosslinking. However, when the concentration of PEG4Tz was manipulated, the resulting degree of stiffening became significantly different between groups, as shown in Figure 4.8. Although 0.5

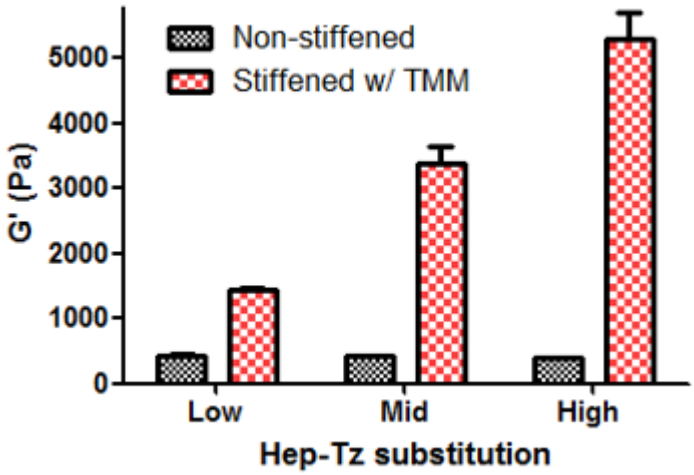

Fig. 4.9. **Tuning stiffening of PEG8NB (3 wt%) hydrogels via manipulating Tz-substitution on Hep-Tz.** PEG4SH: 0.8 wt% (R=0.33); LAP: 4 mM; Visible light intensity: 70 kLux; Polymerization time: 5-minutes

wt% and 1 wt% PEG4Tz stiffening did not result in statistically significant differences in stiffening, this is very likely attributed to the vast reduction in geometry for the 1 wt% condition. The greater the stiffening, the smaller the hydrogels became, both in thickness and in diameter. This caused practical issues when testing them on the rheometer, as they were all initially fabricated with dimensions of 8 mm diameter and 1 mm thickness, but after stiffening with 1 wt% PEG4Tz, the diameter and thickness had nearly halved. This left large gaps between the rheometer base plate and the rheometry head, meaning that the recorded stiffness values were underestimated owing the smaller size of the gels compared to the testing geometry.

Additionally, manipulation of the Tz substitution within the TMMs resulted in significantly different stiffening capabilities while using the same 0.5 wt% TMM, as indicated in Figure 4.9. In low substitution Hep-Tz, there was a less than 4-fold increase in stiffness. In mid substitution Hep-Tz, there was a less than 7-fold increase in stiffness. In high substitution Hep-Tz there was a greater than 10-fold increase in stiffness. Thus, via manipulation of the concentration of TMM (with the same substi-

tution) or the substitution of Tz within the TMM (utilizing the same concentration of TMM) tuning of stiffening was achieved within this system. However, because this system is PEG-based, it would need to be further modified with cell-attachment and MMP-degradable sequences to become biologically relevant. In lieu of this and the understanding that click Tz-NB stiffening is possible within PEG-based, but not gelatin-based hydrogels, a PEG-gelatin hybrid hydrogel system was fabricated, in which temporally-based stiffening capabilities were explored, as shown in Figure 4.10 and Figure 4.11.

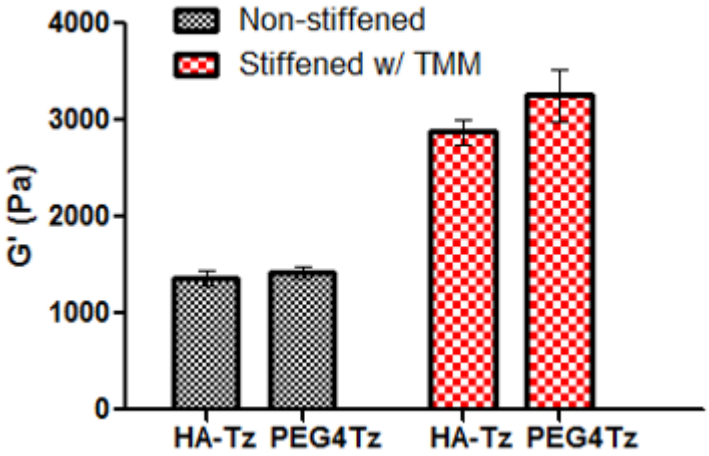

Fig. 4.10. **Effect of TMM (0.5 wt%) on crosslinking of PEG8NB (2 wt%) and Gel(B)NB (0.5 wt%) hydrogels.** PEG4SH: 0.9 wt% (R=0.5); LAP: 4 mM; Visible light intensity: 70 kLux; Polymerization time: 5-minutes

Utilizing a predominately PEG-based hydrogel for stiffening capabilities, while including gelatin for cell-attachment and MMP-degradable sequences, stiffening with HA-Tz and PEG4Tz was accomplished in a physiologically relevant manner. Additionally, it was proven that temporal control of stiffening is possible through simply removing the hydrogels from solution containing TMMs (Figure 4.11). The initial stiffness of the fabricated hydrogels were mimetic of healthy pancreatic tissue, while the 0.5 wt% TMM stiffened hydrogels were mimetic of diseased pancreatic tissue [17].

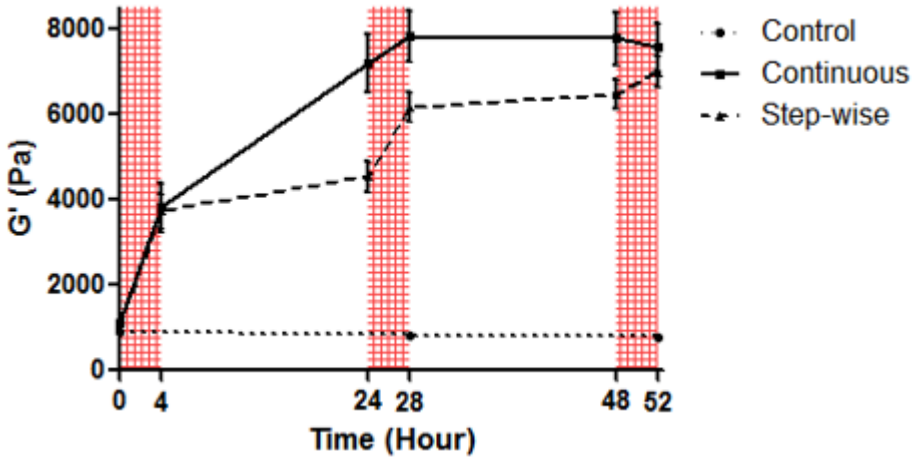

Fig. 4.11. **Temporal control of stiffening of PEG8NB (2 wt%) and Gel(B)NB (0.5 wt%) via PEG4Tz (0.9 wt%).** PEG4SH: 0.9 wt% (R=0.5); LAP: 4 mM; Visible light intensity: 70 kLux; Polymerization time: 5-minutes

Thus, this system along with the method of stiffening was an attractive means to mimic the progression of PDAC, in which matrix stiffness increases and there is an increase in the presence of HA [20]. Verification that TMMs were the cause of stiffening was confirmed qualitatively utilizing DMMB and Hep-Tz stiffening PEG-based hydrogels, as shown in Figure 4.12. Specifically, DMMB selectively binds to sulfated groups, which are naturally present in heparin. When DMMB binds to sulfated groups, it undergoes a color change from blue to pink. Thus, it was confirmed that Hep-Tz was immobilized within the hydrogel due to the selective color change of the stiffened hydrogel.

4.5 Dynamic stiffening of gelatin-based hydrogels via hydrazone crosslinks

Utilizing hydrogels formed with excess CDH for click reaction with aldehyde in oxidized macromers, an additional dynamic stiffening method was explored. First, the efficacy of oHA stiffening was explored with PEG-gelatin hydrogels initially formed via hydrazone crosslinks (Figure 4.13). Again, although gelatin naturally has cell-

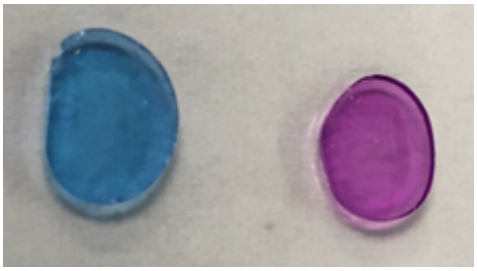

Fig. 4.12. **DMMB-stained PEG-based hydrogels.** PEG4Tz stiffening (left); Hep-Tz stiffening (right)

attachment and MMP-degradable sequences, the presence of NB left potential for further modification of this system utilizing photo-click thiol-norbornene crosslinks from thiol-containing modifiers.

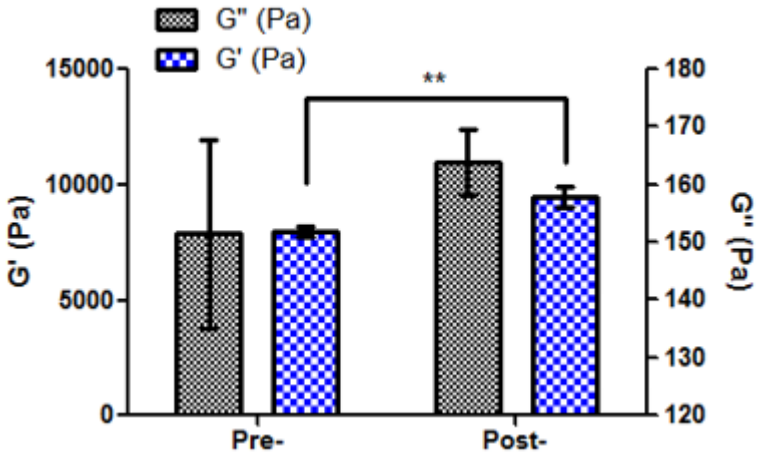

Fig. 4.13. **Effect of 74 kDa 20% oHA (0.5 wt%) on Gel(B)NB-CDH (5 wt%) hydrogel crosslinking.** PEG4pAld: 3.9 wt% (Q=0.5)

Due to the reversible, viscoelastic nature of hydrazone crosslinks and their utilization in shear-thinning, injectable, and self-healing hydrogels [34,48,55,60,61], loss modulus changes were investigated along with storage modulus changes in the stiffening process. Hydrogels initially formed with hydrazone crosslinks were relatively stiff (i.e. 8 kPa storage modulus), when compared to healthy pancreatic tissue [17].

There was significant stiffening from 24-hour exposure to 74 kDa 20% oHA. However, the degree of stiffening along with the initial modulus of this hydrogel made it unattractive for mimicking the progression of PDAC. Utilizing a lower macromer concentration as well as Q-value (i.e. [Ald]:[CDH]), stiffening capabilities of low MW oHA (LMWoHA), mid MW oHA (MMWoHA), oDex, and PEG4Tz were explored, as shown in Figure 4.14.

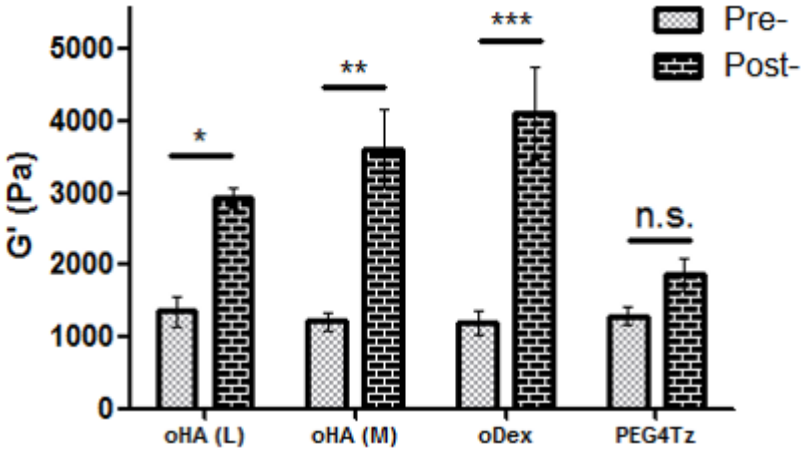

Fig. 4.14. **Tuning stiffening of Gel(B)NB-CDH hydrogels via different oxidized molecules (0.5 wt%) and PEG4Tz (0.5 wt%).** PEG4pAld: 1.3 wt% (R=0.33); oHA (L):14.8 kDa; oHA (M):74 kDa; oDex:100 kDa

Pre-stiffened hydrogels were all formed with the same macromer content and therefore had similar initial moduli. LMWoHA, MMWoHA, and oDex all induced significant stiffening for this hydrogel formulation. However, the stiffening was not significantly different between these three groups. As expected, PEG4Tz was unable to stiffen this gelatin-based hydrogel network, as seen in past results. The initial and stiffened storage moduli of the hydrogels within the LMWoHA, MMWoHA, and oDex groups were attractive because of their physiological relevance to healthy and diseased pancreatic tissue, respectively [17]. Those within the LMWoHA and MMWoHA groups were particularly appealing, as the dynamic increases in both stiffness and HA content mimic the progression of PDAC microenvironment [20]. However,

these hydrogels, with initial networks prepared via click hydrazone chemistry, were extremely sticky, difficult to handle, and became too soft for prolonged cell culturing experiments by the 3rd day. Therefore, primary networks formed from UV-light initiated thiol-norbornene crosslinks and their ability to be controllably stiffened via LMWoHA and MMWoHA were explored. The tunability of stiffening was explored via manipulation of photo-initiator concentration within the gel precursor solution (Figure 4.15) and the concentration of LMWoHA (Figure 4.16).

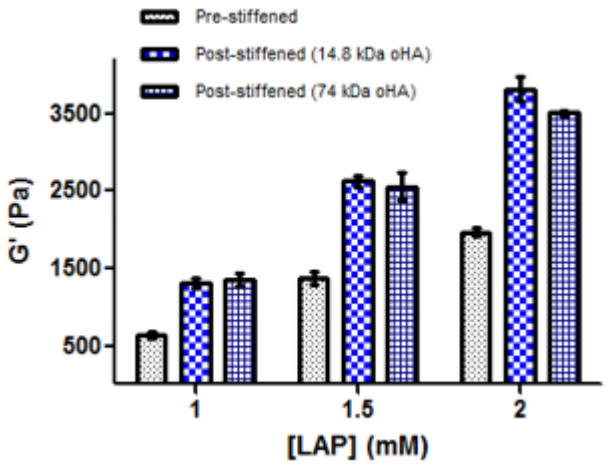

Fig. 4.15. **Tuning oHA (0.5 wt%) stiffening of Gel(B)NB-CDH (5 wt%) hydrogels via manipulation of LAP concentration.** PEG4SH: 1 wt% (R=0.5); UV light intensity: 5 mW/cm^2; Polymerization time: 2-minutes

Similar to increasing the R-value of hydrogels in previous experiments, increasing the concentration of LAP within the gel precursors ultimately led to increased crosslinking density between thiol and norbornene moieties. Due to this, it was expected and observed that the initial storage moduli for hydrogels would be a function of LAP concentration (Figure 4.15). However, in this system the degree of stiffening did not rely on excess NB, as it did in the dynamically stiffened Tz-NB system. Thus, independent of LAP concentration, there was a 2-fold increase in stiffness due to 24-hour incubation with 0.5 wt% LMWoHA or MMWoHA. Increasing the concentration of oHA from 0.5 to 1 wt% did not significantly affect the degree of stiffening (Figure

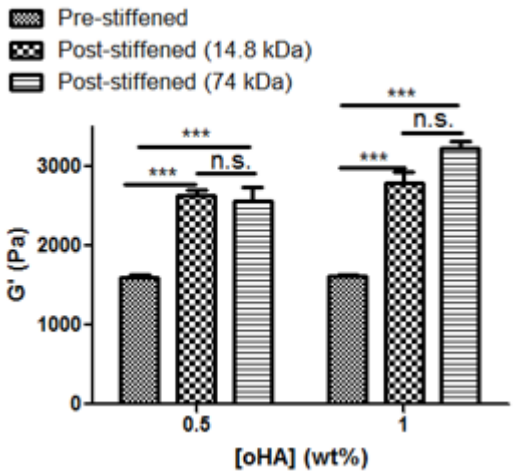

Fig. 4.16. **Effect of varied oHA concentrations on Gel(B)NB-CDH (5 wt%) hydrogel crosslinking.** PEG4SH: 1 wt% (R=0.5); UV light intensity: 5 mW/cm^2; Polymerization time: 2-minutes

4.16). In both conditions, there is excess aldehyde compared to CDH. However, due to the irregularity of the naturally derived materials, it was considered that there would be a difference in stiffening when creating conditions of greater excess. This was not the case.

4.6 Cytotoxicity of HA derivatives

There were two dynamic stiffening chemistries (i.e. Tz-NB and hydrazone click chemistries) utilized in this study that could mimic the progression of PDAC. However, cytotoxicity is always a concern when introducing chemically modified molecules to cells in culture. Thus, cytotoxicity studies with PANC-1 and HA-Tz or oHA were conducted, in which the maximum concentration utilized was the concentration that would (generally) be used for stiffening. The results of the cytotoxicity studies with HA-Tz or oHA can be seen in Figure 4.17 or 4.18, respectively.

It is clear that HA-Tz has a detrimental effect on PANC-1 cells at the concentration intended for stiffening of hydrogels with encapsulated cells (i.e. 0.5 wt%).

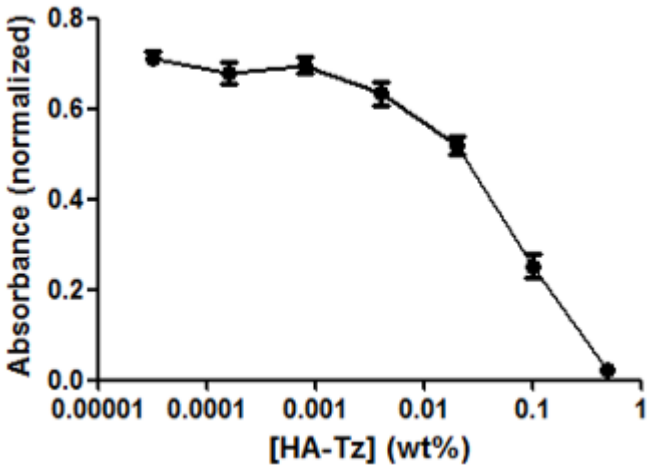

Fig. 4.17. **Effect of various HA-Tz concentrations on PANC-1 metabolic activity**

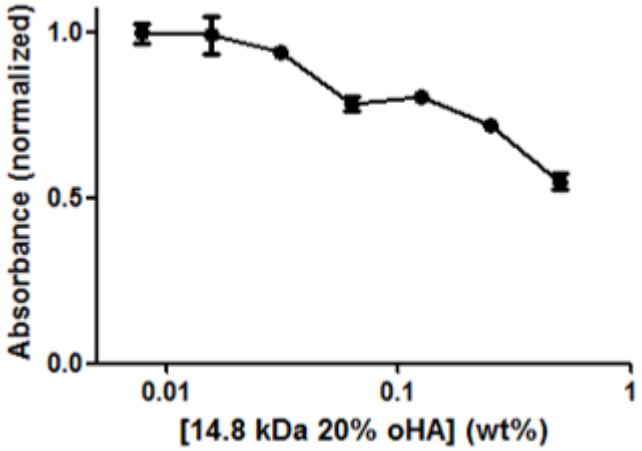

Fig. 4.18. **Effect of various oHA concentrations on PANC-1 metabolic activity**

The LD50 concentration is roughly 10-fold lower than the concentration of HA-Tz that would be used for dynamic stiffening and mimetics of PDAC progression. On the other hand, the LD50 concentration of LMWoHA was not reached when utilizing concentrations up to the dynamic stiffening concentration. Thus, oHA was deemed the appropriate chemical tool for mimicking the progression of PDAC.

4.7 PANC-1 encapsulation, viability, and morphology analysis in PDAC-mimetic hydrogels

Although HA-Tz was deemed to be cytotoxic in 2D, there was potential that the effects in a 3D setting would be different. Utilizing a PEG-gelatin hydrogel, PANC-1 was encapsulated and experienced PDAC-mimetics through dynamic stiffening and HA accumulation (Figure 4.19).

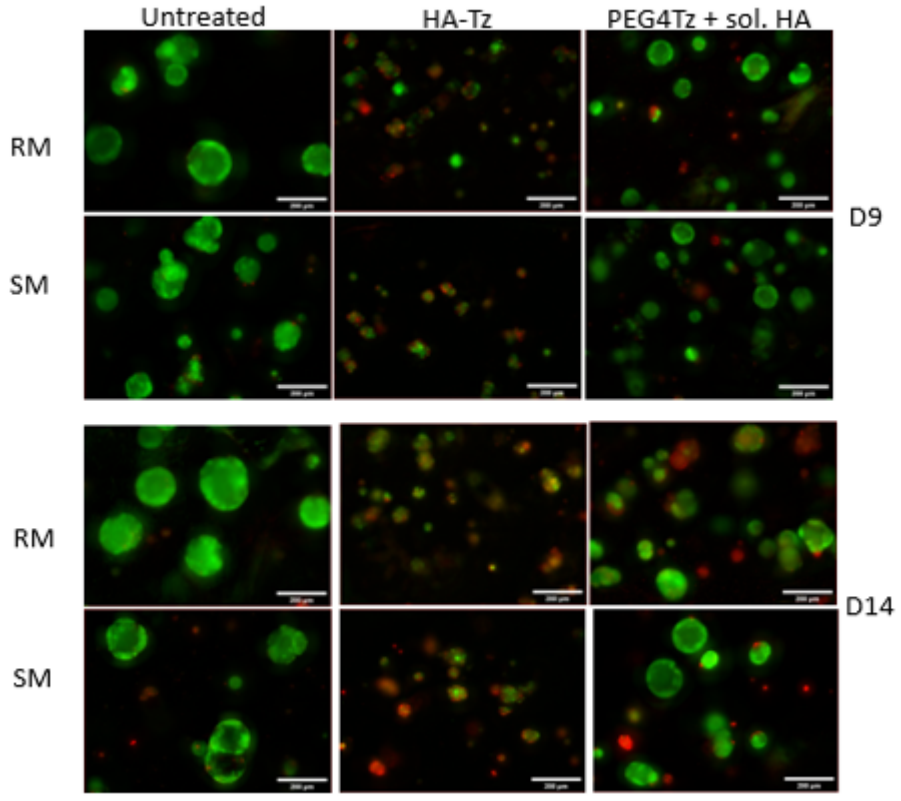

Fig. 4.19. **Effect of culture mediums and stiffening methods on PANC-1 cell viability in PEG8NB (2 wt%) and Gel(B)NB (0.5 wt%) hydrogels.** PEG4SH: 0.9 wt% (R=0.5); LAP: 4 mM; Visible light intensity: 70 kLux; Polymerization time: 5-minutes; TMM: 0.5 wt%; Soluble HA: 0.5 wt%; 24-hour stiffening occurred 7-days after encapsulation; Live (green) stain: Calcien AM; Dead (red) stain: Ethidium III

Hydrogel stiffening was initiated on Day 7 with 0.5 wt% HA-Tz or PEG4Tz. After Tz-mediated stiffening, soluble LMWHA was introduced to the PEG4Tz stiffened

gels to mimic stiffening with presence of HA (although the HA in this case was soluble and not immobilized, like HA-Tz was). Additionally, there was a side-by-side comparison of the cells grown in regular media (RM) or spheroid media (SM). SM results in tumorsphere formation enriched with CSCs that are less metabolically active in response to stressors and more resistant to chemotherapeutics, such as GEM [58]. Regardless of the culture medium, HA-Tz had a detrimental effect on the viability and size of cells as early as 2 days after stiffening. PEG4Tz-stiffened gels also had more dead cells than the non-treated control did, as well as smaller spheroids, but they continued to grow past Day 14. Interestingly, PEG4Tz appeared to be less cytotoxic than HA-Tz. Nonetheless, HA-Tz was verified to be extremely cytotoxic and detrimental to encapsulated cells, at concentrations intended for hydrogel stiffening, and was moved on from.

Next, utilizing another PEG-gelatin hydrogel, PANC-1 was encapsulated and the system was dynamically stiffened via 0.5 wt% LMWoHA or MMWoHA for mimetics of PDAC progression. In Figure 4.20, the viability and morphology results from Day 1 stiffening of the PEG-gelatin system are shown.

Drastically different than 0.5 wt% HA-Tz stiffening, 0.5 wt% LMWoHA or MMWoHA stiffening did not result in different levels of viability qualitatively (live/dead) or quantitatively (alamarblue). Additionally, after stiffening there was not a significant difference in spheroid size. Due to the sticky nature of these hydrogels and their relatively quick degradation, they became too difficult to handle by the 5^{th} day of encapsulation. Thus, an increased concentration of LAP (i.e. 1.5 mM) was utilized to form the same composition of hydrogel for increased integrity and prolonged cell study potential. Stiffening was accomplished via MMWoHA at concentrations of 0.5 or 1 wt% (Figure 4.21).

Utilizing 1.5 mM LAP in the gel precursor, as opposed to 1 mM LAP, increased the longevity of these hydrogels and thus their cell culture capabilities. After 24-hour stiffening with 0.5 or 1 wt% LMWoHA, gels were imaged. Additionally, 4- and 7- days after stiffening was completed (Day 6 and 9, respectively), these gels were imaged.

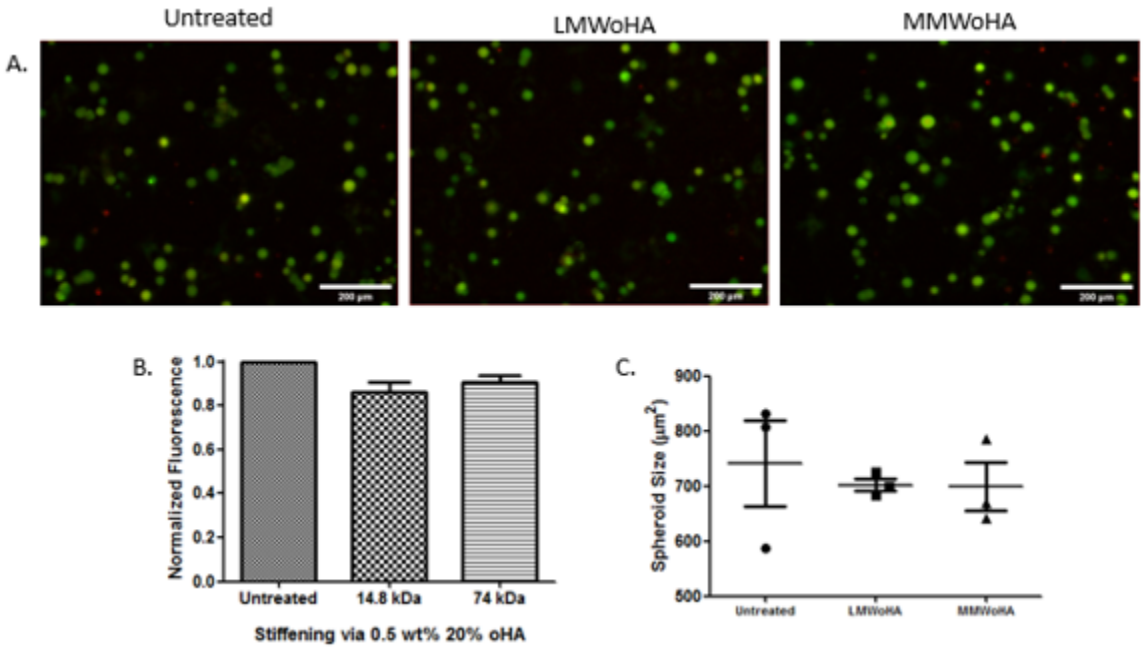

Fig. 4.20. **Live/dead staining (A), metabolic activity (B), and spheroid sizes (C) of PANC-1 in Gel(B)NB-CDH (5 wt%) hydrogels following oHA (0.5 wt%) stiffening.** PEG4SH: 1 wt% (R=0.5); LAP: 1 mM; UV light intensity: 5 mW/cm^2; Polymerization time: 2-minutes. LMWoHA: 14.8 kDa; MMWoHA: 74 kDa; 24-hour stiffening occurred 1-day after encapsulation; Live (green) stain: Calcien AM; Dead (red) stain: Ethidium III; images taken and alamarblue conducted on Day 2

On the day stiffening was completed (Day 2), there was no significant difference in spheroid size or viability. By the 6th day (i.e. 4-days after stiffening), there was a significant difference between the sizes of the spheroids in the gels that were stiffened by 0.5 or 1 wt% LMWoHA. By the 9th day (i.e. 7-days after stiffening), there was no longer a significant difference in spheroid size between the stiffened groups.

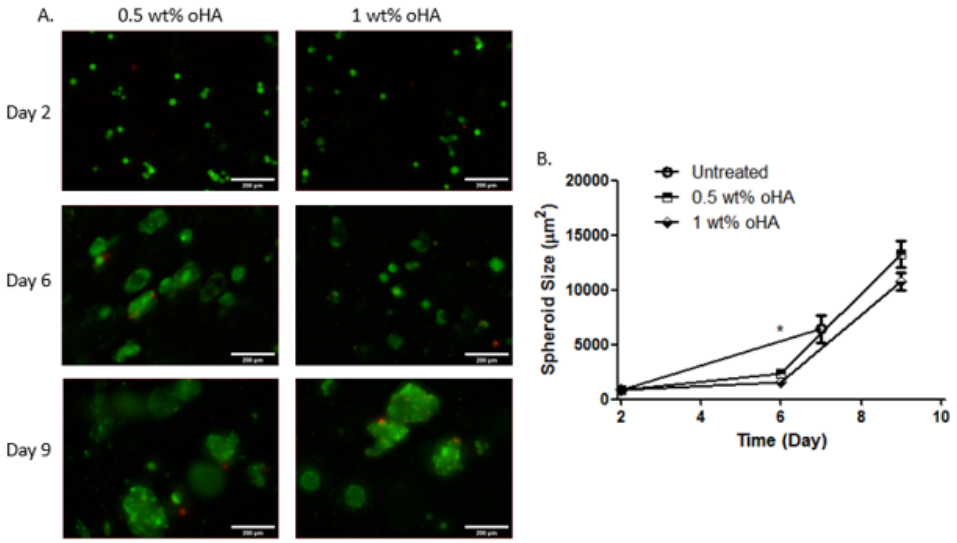

Fig. 4.21. **Live/dead staining (A) and spheroid sizes (B) of PANC-1 in Gel(B)NB-CDH (5 wt%) hydrogels following stiffening with oHA (0.5 or 1 wt%).** PEG4SH: 1 wt% (R=0.5); LAP: 1.5 mM; UV light intensity: 5 mW/cm^2; Polymerization time: 2-minutes; 24-hour stiffening occurred 1-day after encapsulation (Day 2)

4.8 Response of encapsulated PANC-1 to chemotherapeutics in PDAC-mimetic hydrogels

PEG-gelatin hybrid hydrogels were stiffened via 1 wt% MMWoHA on the 7th day of encapsulation, followed by initiation of 1 μM gemcitabine treatment on the 8th day. Drug treatment endured for 4-days (i.e. until Day 12). Before and after stiffening and drug treatment, alamarblue was conducted. A baseline for metabolic activity was quantified via alamarblue before stiffening and drug treatment. The results from this study are shown in Figure 4.22.

On Day 7, encapsulated PANC-1 were viable and had formed spheroids. Overnight stiffening with 1 wt% MMWoHA resulted in a significant decrease in metabolic activity, according to alamarblue assay. Following alamarblue assay, on Day 8, 1 μM GEM was added to wells with non-stiffened and stiffened gels. Control non-stiffened

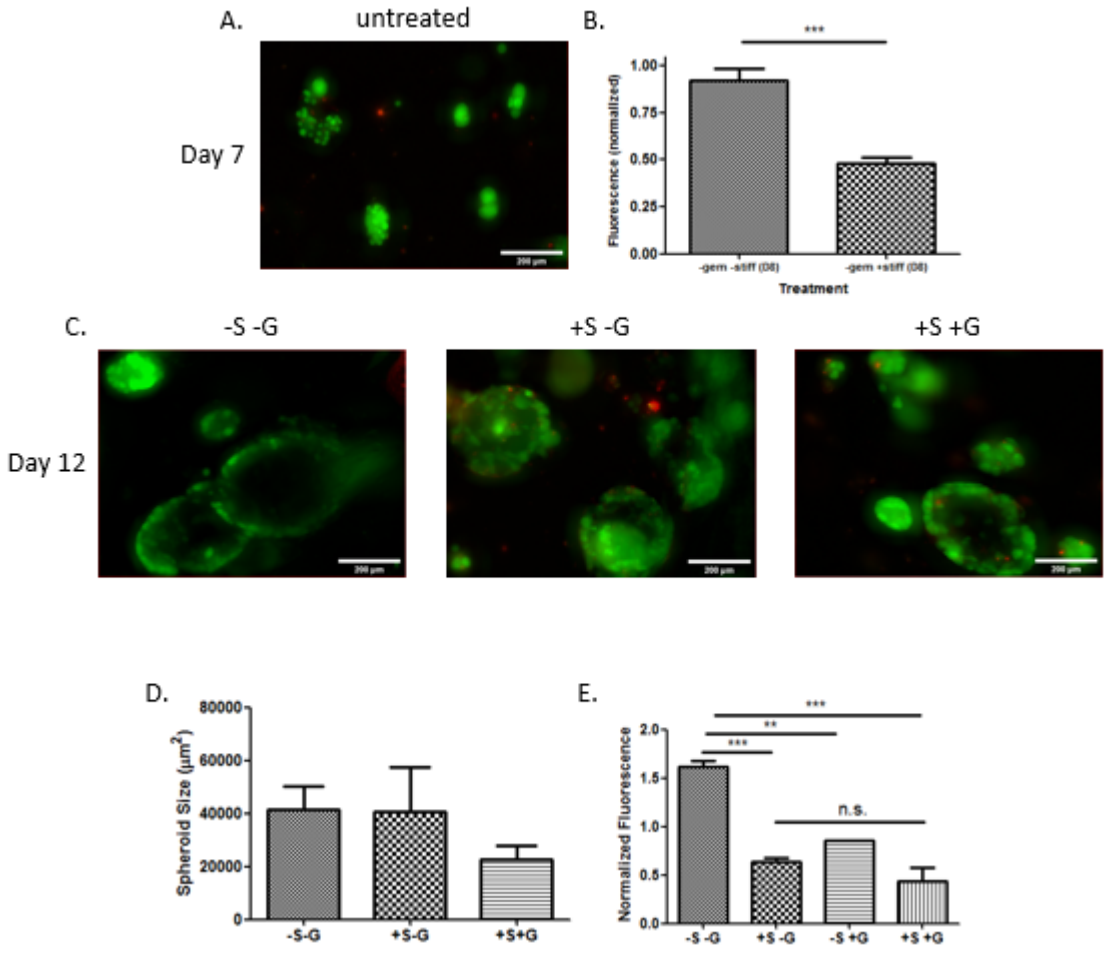

Fig. 4.22. **Live/dead staining (A and C), metabolic activity (B and E), and spheroid sizes (D) of PANC-1 in Gel(B)NB-CDH (5 wt%) hydrogels following oHA (1 wt%) stiffening and GEM (1 μM) treatment.** PEG4SH: 1 wt% (R=0.5); LAP: 1.5 mM; UV light intensity: 5 mW/cm^2; Polymerization time: 2-minutes. 24-hour stiffening occurred 7-days after encapsulation; 4-day GEM treatment started immediately after stiffening; metabolic activity determined via alamarblue following stiffening (Day 8) and GEM treatment (Day 12); Live (green) stain: Calcien AM; Dead (red) stain: Ethidium III. -S -G: non-stiffened and non-treated; -S +G: non-stiffened and GEM-treated; +S -G: HA-stiffened and non-treated; +S +G: HA-stiffened and GEM-treated

and stiffened conditions were not treated with GEM. After 4-days of GEM treatment, live/dead and alamarblue assay were completed. By the end of GEM treat-

ment (Day 12), PANC-1 spheroids in all conditions had insignificant size differences and viabilities (non-stiffened/GEM-treated hydrogels were too soft and unworkable). Metabolic activities in non-stiffened/non-treated and non-stiffened/treated groups were significantly different. However, metabolic activities in stiffened/non-treated and stiffened/GEM-treated groups were not significantly different. This suggests that the synergistic effect of stiffening with HA increases drug resistance. Although there was a decrease in metabolic activity, the viability of imaged cells was similar. Therefore, another experiment was conducted in which the concentration of GEM was increased. Additionally, the concentration of LAP in the gel precursor was increased to 2 mM, raising the non-stiffened and stiffened moduli by greater than 40%. This ensured that the gels would remain workable for the duration of the study.

Immediately following stiffening (Day 2), there was not a significant difference between spheroid sizes or viabilities between the control and the stiffened conditions. Two days after the gels were stiffened (Day 4), 4-day GEM treatment started. Immediately following GEM treatment (Day 8), spheroids in the non-stiffened/non-treated gels were significantly larger than all other conditions; there was no significant difference between spheroid sizes in the remaining conditions. The viability of encapsulated cells was comparable between all conditions. Not surprisingly, there were more dead cells within the GEM-treated gels than the non-treated gels. Additionally, metabolic activity of cells within the non-stiffened/non-treated gels were significantly different than those within the PEG-stiffened/GEM-treated gels; there was no significant difference between metabolic activities in any other conditions.

Binding interactions between HA and CD44 activate and regulate several cellular signaling processes which are key in the mediation of tumor progression, metastasis, and chemoresistance [62]. To investigate whether HA binding interactions played a role in drug resistance, encapsulated cells were fixed following GEM treatment and subsequently stained for CD44. An increase in CD44 expression for cells in HA-stiffened/GEM-treated hydrogels would suggest a vital role of HA-binding in drug resistance. Interestingly, CD44 expression was the highest in the non-stiffened/non-

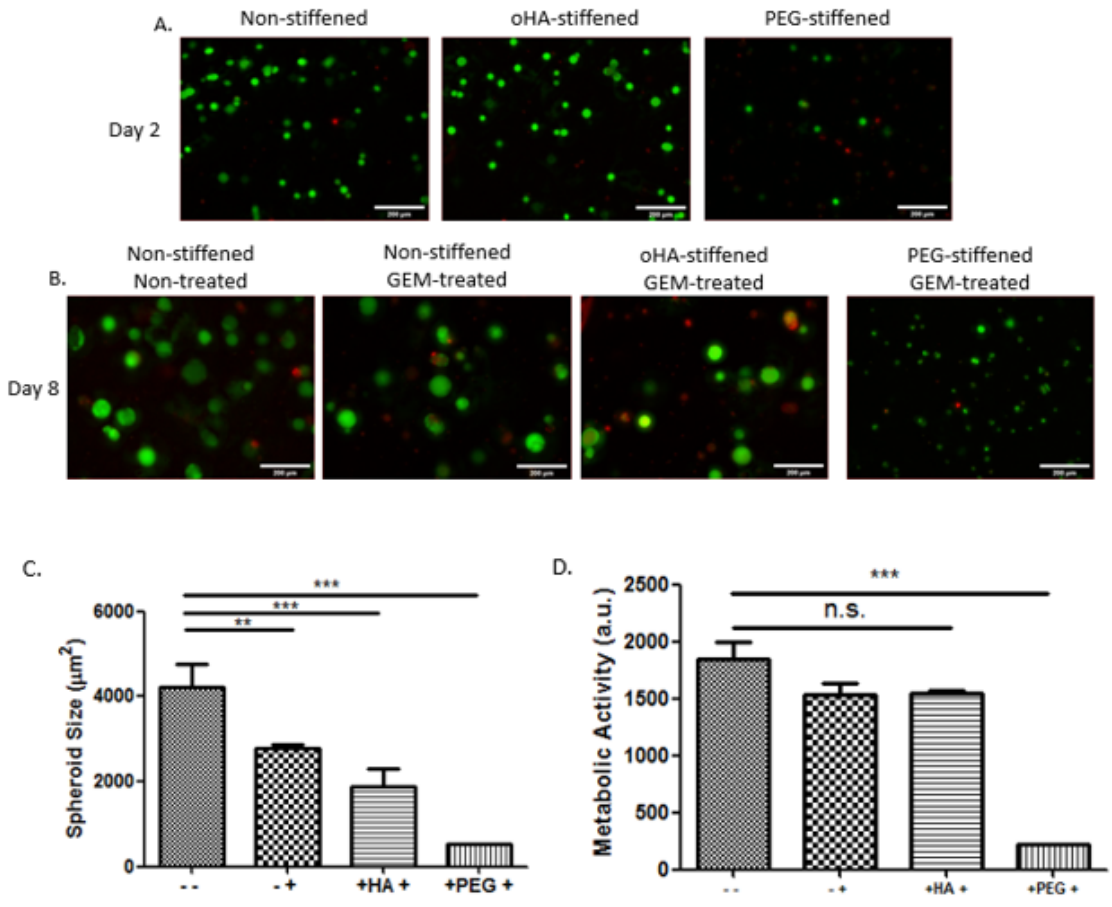

Fig. 4.23. **Day 2 (A) and Day 8 (B) live/dead staining of encapsulated PANC-1; Day 8 spheroid size (C) and metabolic activity (D) of encapsulated PANC-1 following stiffening and drug treatment in Gel(B)NB-CDH (5 wt%) hydrogels; Stiffening via oHA (0.5 wt%) or PEG4pAld (0.5 wt%); 4 μM GEM treatment.** PEG4SH: 1 wt% (R=0.5); LAP: 2 mM; UV light intensity: 5 mW/cm^2; Polymerization time: 2-minutes; 24-hour stiffening occurred 1-day after encapsulation (Day 2); 4-day GEM treatment started 2-days after stiffening (Day 4); metabolic activity determined via alamarblue assay following GEM treatment (Day 8); Live: green; Dead: red; - -: non-stiffened and non-treated; - +: non-stiffened and GEM-treated; +HA +: HA-stiffened and GEM-treated; +PEG +: PEG-stiffened and GEM-treated

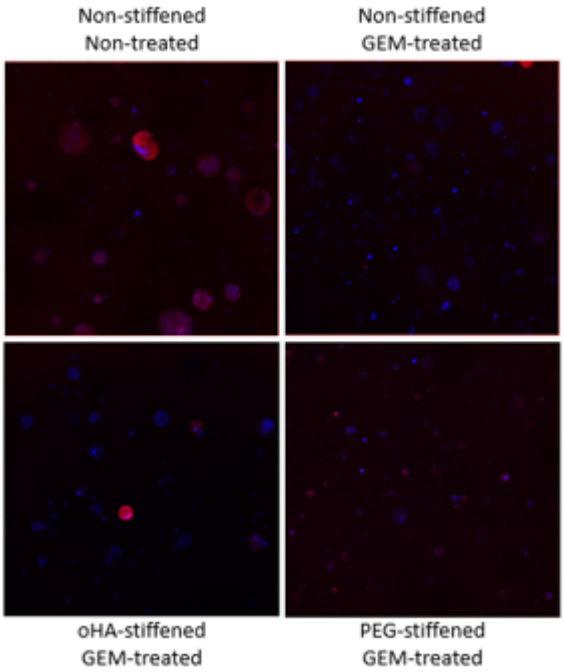

Fig. 4.24. **DAPI and CD44 stained PANC-1 encapsulated in Gel(B)NB-CDH (5 wt%) hydrogels following stiffening and GEM treatment; Stiffening via oHA (0.5 wt%) or PEG4pAld (0.5 wt%); 4 μM GEM treatment.** PEG4SH: 1 wt%; LAP: 2 mM; UV light intensity: 5 mW/cm^2; Polymerization time: 2-minutes; 24-hour stiffening occurred 1-day after encapsulation (Day 2); 4-day GEM treatment started 2-days after stiffening (Day 4); DAPI: blue; CD44: red

treated condition. Very little CD44 was expressed in the remaining, GEM-treated, conditions. GEM may play an antagonistic role in CD44 expression, which would be a novel discovery. Therefore, a similar experiment was conducted in which the GEM concentration was increased further, to see more significant cell death, as well as introducing oHA-stiffened/non-treated and PEG-stiffened/non-treated groups.

Immediately following stiffening (Day 2), spheroid sizes in the stiffened groups were similar, but significantly different than the non-stiffened group. Again, 4-day GEM treatment started two days after stiffening (Day 4). Immediately following GEM-treatment (Day 8), spheroid sizes in the non-stiffened/non-treated and HA-stiffened

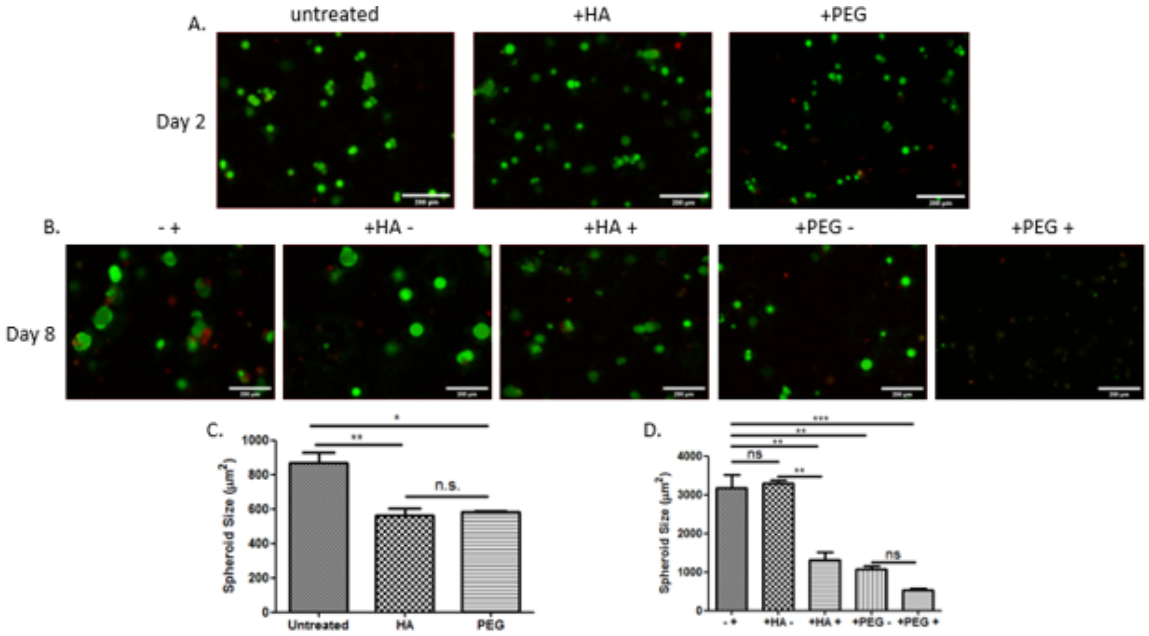

Fig. 4.25. **Day 2 (A) and Day 8 (B) live/dead staining of encapsulated PANC-1; Day 2 (C) and Day 8 (D) spheroid sizes of PANC-1; Gel(B)NB-CDH (5 wt%) hydrogels stiffened via oHA (0.5 wt%) or PEG4pAld (0.25 wt%); treated with 10 μM GEM.** PEG4SH: 1 wt% (R=0.5); LAP: 2 mM; UV light intensity: 5 mW/cm^2; Polymerization time: 2-minutes. 24-hour stiffening occurred 1-day after encapsulation (Day 2); 4-day GEM treatment started 2-days after stiffening (Day 4); metabolic activity determined via alamarblue following GEM treatment (Day 8); Live: green; Dead: red; - +: non-stiffened and GEM-treated; +HA: HA-stiffened; +PEG: PEG-stiffened; +HA -: HA-stiffened and non-treated; +HA +: HA-stiffened and GEM-treated; +PEG -: PEG-stiffened and non-treated +PEG +: PEG-stiffened and GEM-treated

/non-treated groups were significantly larger than those in all other groups. There was no significant difference between spheroid sizes in PEG-stiffened/non-treated and PEG-stiffened/GEM-treated groups. Interestingly, the most dead cells were in the non-stiffened/GEM-treated and PEG-stiffened/GEM-treated conditions. It is clear that HA-stiffening allows cells to continue to grow normally, whereas PEG-stiffening does not. Additionally, cells within HA-stiffened/GEM-treated gels had similar via-

bility to those within HA-stiffened/non-treated gels. There was a clear difference between viabilities in PEG-stiffened/non-treated and PEG-stiffened/GEM-treated conditions. Contrarily, when PANC-1 was cultured in stiff hydrogels and treated with an antitumor peptide drug, in the absence of HA, there was extremely low viability [63]. This suggests that HA-stiffening promotes PDAC cell growth and survival, even in the presence of chemotherapeutics, similar to the effects of matrix stiffening and HA accumulation in PDAC progression.

5. CONCLUSION AND RECOMMENDATION FOR FUTURE WORK

In this study, dynamically tunable hydrogels mimicking the development of PDAC (i.e. increased matrix stiffness and HA accumulation) were developed. Specifically, (1) PEG-gelatin hybrid hydrogel initially formed with photo-click thiol-norbornene crosslinks containing unreacted norbornene for further click crosslinking with tetrazine-modified HA and (2) PEG-gelatin hybrid hydrogel initially formed with click hydrazone or photo-click thiol-norbornene crosslinks containing unreacted carbohydrazide for further crosslinking with oxidized HA. It was determined that tetrazine-modified HA is cytotoxic at concentrations below that intended for hydrogel stiffening. Thus, oxidized HA was utilized with PEG-gelatin hybrid hydrogels containing excess carbohydrazide for PDAC-mimetics. This system was utilized for PANC-1 cell encapsulation and did not result in significantly different levels of viability or metabolic activity, when stiffened with 0.5 wt% LMWoHA or MMWoHA. Furthermore, due to stiffening there was an increase in drug resistance for cells encapsulated in hydrogels stiffened with oxidized HA. This resistance mimics the behavior of PDAC cells in their natural environment during disease progression and, therefore, is an attractive culture platform for studying the interactions of PDAC cells with their environment and the resistance of drugs.

Moving forward, it is recommended that a system is developed in which HA is initially present and is further concentrated due to stiffening. This would more accurately mimic the progression of PDAC, as healthy pancreatic tissue has HA as well. Another benefit of using dynamic hydrazone bonds are their innate reversibility and viscoelasticity. Thus, working to characterize and tune not only stiffness, but viscoelasticity is of great interest, considering the viscoelastic nature of tissue. Additionally, stiffening with oxidized HA should be accomplished with concentrations less

than 1 wt% because 0.5 and 1 wt% oxidized HA stiffen the network similarly and 1 wt% makes the encapsulated cells less metabolically active. To investigate how important HA is in increasing drug resistance, blocking HA binding with a peptide could be explored. Additionally, comparison of CD44 expression between HA-stiffened/non-treated and HA-stiffened/GEM-treated groups could provide insight into the importance of HA-CD44 binding interactions. Alongside drug studies, detection of EMT markers, such as N-cadherin on PDAC cells, or the expression of αSMA in PSCs could be visited, as they are generally correlated with worsened prognosis and more invasive cancers.

REFERENCES

REFERENCES

[1] Q. Zhou and D. A. Melton, "Author correction: Pancreas regeneration," *Nature*, vol. 560, no. 7720, p. E34.

[2] R. L. Siegel, K. D. Miller, and A. Jemal, "Cancer statistics, 2019," *CA Cancer J Clin*, vol. 69, no. 1, pp. 7–34, 2019.

[3] S. K. Dougan, "The pancreatic cancer microenvironment," *Cancer J*, vol. 23, no. 6, pp. 321–325, 2017.

[4] A. Y. L. Lee, C. L. Dubois, K. Sarai, S. Zarei, D. F. Schaeffer, M. Sander, and J. L. Kopp, "Cell of origin affects tumour development and phenotype in pancreatic ductal adenocarcinoma," *Gut*, 2018.

[5] Y. Shichi, N. Sasaki, M. Michishita, F. Hasegawa, Y. Matsuda, T. Arai, F. Gomi, J. Aida, K. Takubo, M. Toyoda, H. Yoshimura, K. Takahashi, and T. Ishiwata, "Enhanced morphological and functional differences of pancreatic cancer with epithelial or mesenchymal characteristics in 3d culture," *Sci Rep*, vol. 9, no. 1, p. 10871, 2019.

[6] F. Quinonero, C. Mesas, K. Doello, L. Cabeza, G. Perazzoli, C. Jimenez-Luna, A. Rosa Rama, C. Melguizo, and J. Prados, "The challenge of drug resistance in pancreatic ductal adenocarcinoma: a current overview," *Cancer Biol Med*, vol. 16, no. 4, pp. 688–699, 2019.

[7] T. Seufferlein and T. J. Ettrich, "Treatment of pancreatic cancer-neoadjuvant treatment in resectable pancreatic cancer (pdac)," *Transl Gastroenterol Hepatol*, vol. 4, p. 21, 2019.

[8] T. Seufferlein, "Systemic treatment of advanced pancreatic cancer–step by step progress," *Gut*, vol. 62, no. 5, pp. 660–1, 2013.

[9] T. Seufferlein, G. von Wichert, and G. Adler, "[palliative treatment of pancreatic cancer]," *Dtsch Med Wochenschr*, vol. 132, no. 15, pp. 813–7, 2007.

[10] A. Kowalewski, L. Szylberg, M. Saganek, W. Napiontek, P. Antosik, and D. Grzanka, "Emerging strategies in brca-positive pancreatic cancer," *J Cancer Res Clin Oncol*, vol. 144, no. 8, pp. 1503–1507, 2018.

[11] C. Bonnans, J. Chou, and Z. Werb, "Remodelling the extracellular matrix in development and disease," *Nat Rev Mol Cell Biol*, vol. 15, no. 12, pp. 786–801, 2014.

[12] A. D. Theocharis, S. S. Skandalis, C. Gialeli, and N. K. Karamanos, "Extracellular matrix structure," *Adv Drug Deliv Rev*, vol. 97, pp. 4–27, 2016.

[13] N. Davidenko, C. F. Schuster, D. V. Bax, R. W. Farndale, S. Hamaia, S. M. Best, and R. E. Cameron, "Correction to: Evaluation of cell binding to collagen and gelatin: a study of the effect of 2d and 3d architecture and surface chemistry," *J Mater Sci Mater Med*, vol. 29, no. 4, p. 39, 2018.

[14] K. M. Mabry, R. L. Lawrence, and K. S. Anseth, "Dynamic stiffening of poly(ethylene glycol)-based hydrogels to direct valvular interstitial cell phenotype in a three-dimensional environment," *Biomaterials*, vol. 49, pp. 47–56, 2015.

[15] V. Irawan, A. Higuchi, and T. Ikoma, "Physical cues of biomaterials guide stem cell fate of differentiation: The effect of elasticity of cell culture biomaterials," *Open Physics*, vol. 16, no. 1, pp. 943–955, 2018.

[16] O. Chaudhuri, L. Gu, D. Klumpers, M. Darnell, S. A. Bencherif, J. C. Weaver, N. Huebsch, H. P. Lee, E. Lippens, G. N. Duda, and D. J. Mooney, "Hydrogels with tunable stress relaxation regulate stem cell fate and activity," *Nat Mater*, vol. 15, no. 3, pp. 326–34, 2016.

[17] A. J. Rice, E. Cortes, D. Lachowski, B. C. H. Cheung, S. A. Karim, J. P. Morton, and A. Del Rio Hernandez, "Matrix stiffness induces epithelial-mesenchymal transition and promotes chemoresistance in pancreatic cancer cells," *Oncogenesis*, vol. 6, no. 7, p. e352, 2017.

[18] M. Weniger, K. C. Honselmann, and A. S. Liss, "The extracellular matrix and pancreatic cancer: A complex relationship," *Cancers (Basel)*, vol. 10, no. 9, 2018.

[19] S. Nallanthighal, J. P. Heiserman, and D. J. Cheon, "The role of the extracellular matrix in cancer stemness," *Front Cell Dev Biol*, vol. 7, p. 86, 2019.

[20] N. Sato, S. Kohi, K. Hirata, and M. Goggins, "Role of hyaluronan in pancreatic cancer biology and therapy: Once again in the spotlight," *Cancer Sci*, vol. 107, no. 5, pp. 569–75, 2016.

[21] S. Makkar, T. E. Riehl, B. Chen, Y. Yan, D. M. Alvarado, M. A. Ciorba, and W. F. Stenson, "Hyaluronic acid binding to tlr4 promotes proliferation and blocks apoptosis in colon cancer," *Mol Cancer Ther*, vol. 18, no. 12, pp. 2446–2456, 2019.

[22] X. B. Cheng, S. Kohi, A. Koga, K. Hirata, and N. Sato, "Hyaluronan stimulates pancreatic cancer cell motility," *Oncotarget*, vol. 7, no. 4, pp. 4829–40, 2016.

[23] A. Kultti, X. Li, P. Jiang, C. B. Thompson, G. I. Frost, and H. M. Shepard, "Therapeutic targeting of hyaluronan in the tumor stroma," *Cancers (Basel)*, vol. 4, no. 3, pp. 873–903, 2012.

[24] J. Carthew, J. E. Frith, J. S. Forsythe, and V. X. Truong, "Polyethylene glycol-gelatin hydrogels with tuneable stiffness prepared by horseradish peroxidase-activated tetrazine-norbornene ligation," *Journal of Materials Chemistry B*, vol. 6, no. 9, pp. 1394–1401, 2018.

[25] Z. Munoz, H. Shih, and C. C. Lin, "Gelatin hydrogels formed by orthogonal thiol-norbornene photochemistry for cell encapsulation," *Biomaterials Science*, vol. 2, no. 8, pp. 1063–1072, 2014.

[26] M. J. Ware, V. Keshishian, J. J. Law, J. C. Ho, C. A. Favela, P. Rees, B. Smith, S. Mohammad, R. F. Hwang, K. Rajapakshe, C. Coarfa, S. X. Huang, D. P. Edwards, S. J. Corr, B. Godin, and S. A. Curley, "Generation of an in vitro 3d pdac stroma rich spheroid model," *Biomaterials*, vol. 108, pp. 129–142, 2016.

[27] A. Grapin-Botton, "Three-dimensional pancreas organogenesis models," *Diabetes Obes Metab*, vol. 18 Suppl 1, pp. 33–40, 2016.

[28] H. Shih and C. C. Lin, "Visible-light-mediated thiol-ene hydrogelation using eosin-y as the only photoinitiator," *Macromolecular Rapid Communications*, vol. 34, no. 3, pp. 269–273, 2013.

[29] ——, "Photo-click hydrogels prepared from functionalized cyclodextrin and poly(ethylene glycol) for drug delivery and in situ cell encapsulation," *Biomacromolecules*, vol. 16, no. 7, pp. 1915–1923, 2015.

[30] H. Shih, H. Y. Liu, and C. C. Lin, "Improving gelation efficiency and cytocompatibility of visible light polymerized thiol-norbornene hydrogels via addition of soluble tyrosine," *Biomaterials Science*, vol. 5, no. 3, pp. 589–599, 2017.

[31] A. Funfak, L. Bouzhir, E. Gontran, N. Minier, P. Dupuis-Williams, and S. Gobaa, "Biophysical control of bile duct epithelial morphogenesis in natural and synthetic scaffolds," *Front Bioeng Biotechnol*, vol. 7, p. 417, 2019.

[32] R. F. Pereira, C. C. Barrias, P. J. Bartolo, and P. L. Granja, "Cell-instructive pectin hydrogels crosslinked via thiol-norbornene photo-click chemistry for skin tissue engineering," *Acta Biomaterialia*, vol. 66, pp. 282–293, 2018.

[33] K. H. Song, S. J. Heo, A. P. Peredo, M. D. Davidson, R. L. Mauck, and J. A. Burdick, "Influence of fiber stiffness on meniscal cell migration into dense fibrous networks," *Advanced Healthcare Materials*, 2019.

[34] Z. Wei and S. Gerecht, "A self-healing hydrogel as an injectable instructive carrier for cellular morphogenesis," *Biomaterials*, vol. 185, pp. 86–96, 2018.

[35] E. E. Charrier, K. Pogoda, R. G. Wells, and P. A. Janmey, "Control of cell morphology and differentiation by substrates with independently tunable elasticity and viscous dissipation," *Nat Commun*, vol. 9, no. 1, p. 449, 2018.

[36] Y. Tan, H. Huang, D. C. Ayers, and J. Song, "Modulating viscoelasticity, stiffness, and degradation of synthetic cellular niches via stoichiometric tuning of covalent versus dynamic noncovalent cross-linking," *Acs Central Science*, vol. 4, no. 8, pp. 971–981, 2018.

[37] S. Tang, H. Ma, H. C. Tu, H. R. Wang, P. C. Lin, and K. S. Anseth, "Adaptable fast relaxing boronate-based hydrogels for probing cell-matrix interactions," *Adv Sci (Weinh)*, vol. 5, no. 9, p. 1800638, 2018.

[38] K. M. Wisdom, K. Adebowale, J. Chang, J. Y. Lee, S. Nam, R. Desai, N. S. Rossen, M. Rafat, R. B. West, L. Hodgson, and O. Chaudhuri, "Matrix mechanical plasticity regulates cancer cell migration through confining microenvironments," *Nature Communications*, vol. 9, 2018.

[39] K. A. Gunay, T. L. Ceccato, J. S. Silver, K. L. Bannister, O. J. Bednarski, L. A. Leinwand, and K. S. Anseth, "Peg-anthracene hydrogels as an on-demand stiffening matrix to study mechanobiology," *Angew Chem Int Ed Engl*, vol. 58, no. 29, pp. 9912–9916, 2019.

[40] M. G. Ondeck, A. Kumar, J. K. Placone, C. M. Plunkett, B. F. Matte, K. C. Wong, L. Fattet, J. Yang, and A. J. Engler, "Dynamically stiffened matrix promotes malignant transformation of mammary epithelial cells via collective mechanical signaling," *Proceedings of the National Academy of Sciences of the United States of America*, vol. 116, no. 9, pp. 3502–3507, 2019.

[41] R. S. Stowers, S. C. Allen, K. Sanchez, C. L. Davis, N. D. Ebelt, C. Van Den Berg, and L. J. Suggs, "Extracellular matrix stiffening induces a malignant phenotypic transition in breast epithelial cells," *Cellular and Molecular Bioengineering*, vol. 10, no. 1, pp. 114–123, 2017.

[42] M. R. Arkenberg and C. C. Lin, "Orthogonal enzymatic reactions for rapid crosslinking and dynamic tuning of peg-peptide hydrogels," *Biomater Sci*, vol. 5, no. 11, pp. 2231–2240, 2017.

[43] M. R. Arkenberg, D. M. Moore, and C. C. Lin, "Dynamic control of hydrogel crosslinking via sortase-mediated reversible transpeptidation," *Acta Biomater*, vol. 83, pp. 83–95, 2019.

[44] H. Y. Liu, T. Greene, T. Y. Lin, C. S. Dawes, M. Korc, and C. C. Lin, "Enzyme-mediated stiffening hydrogels for probing activation of pancreatic stellate cells," *Acta Biomater*, vol. 48, pp. 258–269, 2017.

[45] C. C. Lin, "Recent advances in crosslinking chemistry of biomimetic poly(ethylene glycol) hydrogels," *RSC Adv*, vol. 5, no. 50, pp. 39 844–398 583, 2015.

[46] N. Gjorevski and M. P. Lutolf, "Synthesis and characterization of well-defined hydrogel matrices and their application to intestinal stem cell and organoid culture," *Nat Protoc*, vol. 12, no. 11, pp. 2263–2274, 2017.

[47] Y. Hao, J. Song, A. Ravikrishnan, K. T. Dicker, E. W. Fowler, A. B. Zerdoum, Y. Li, H. Zhang, A. K. Rajasekaran, J. M. Fox, and X. Jia, "Rapid bioorthogonal chemistry enables in situ modulation of the stem cell behavior in 3d without external triggers," *ACS Appl Mater Interfaces*, vol. 10, no. 31, pp. 26 016–26 027, 2018.

[48] L. Wang, W. F. Zhou, Q. G. Wang, C. Xu, Q. Tang, and H. Yang, "An injectable, dual responsive, and self-healing hydrogel based on oxidized sodium alginate and hydrazide-modified poly(ethyleneglycol)," *Molecules*, vol. 23, no. 3, 2018.

[49] C. C. Lin, C. S. Ki, and H. Shih, "Thiol-norbornene photo-click hydrogels for tissue engineering applications," *J Appl Polym Sci*, vol. 132, no. 8, 2015.

[50] H. Shih, T. Greene, M. Korc, and C. C. Lin, "Modular and adaptable tumor niche prepared from visible light initiated thiol-norbornene photopolymerization," *Biomacromolecules*, vol. 17, no. 12, pp. 3872–3882, 2016.

[51] H. Y. Liu, H. D. Nguyen, and C. C. Lin, "Dynamic peg-peptide hydrogels via visible light and fmn-induced tyrosine dimerization," *Adv Healthc Mater*, vol. 7, no. 22, p. e1800954, 2018.

[52] H. Y. Liu, M. Korc, and C. C. Lin, "Biomimetic and enzyme-responsive dynamic hydrogels for studying cell-matrix interactions in pancreatic ductal adenocarcinoma," *Biomaterials*, vol. 160, pp. 24–36, 2018.

[53] H. Shih and C. C. Lin, "Cross-linking and degradation of step-growth hydrogels formed by thiol-ene photoclick chemistry," *Biomacromolecules*, vol. 13, no. 7, pp. 2003–2012, 2012.

[54] A. C. Knall, M. Hollauf, and C. Slugovc, "Kinetic studies of inverse electron demand diels-alder reactions (iedda) of norbornenes and 3,6-dipyridin-2-yl-1,2,4,5-tetrazine," *Tetrahedron Lett*, vol. 55, no. 34, pp. 4763–4766.

[55] L. S. Wang, J. E. Chung, P. P. Y. Chan, and M. Kurisawa, "Injectable biodegradable hydrogels with tunable mechanical properties for the stimulation of neurogenesic differentiation of human mesenchymal stem cells in 3d culture," *Biomaterials*, vol. 31, no. 6, pp. 1148–1157, 2010.

[56] A. Bauer, L. Gu, B. Kwee, W. A. Li, M. Dellacherie, A. D. Celiz, and D. J. Mooney, "Hydrogel substrate stress-relaxation regulates the spreading and proliferation of mouse myoblasts," *Acta Biomater*, vol. 62, pp. 82–90, 2017.

[57] B. D. Fairbanks, M. P. Schwartz, A. E. Halevi, C. R. Nuttelman, C. N. Bowman, and K. S. Anseth, "A versatile synthetic extracellular matrix mimic via thiol-norbornene photopolymerization," *Advanced Materials*, vol. 21, no. 48, pp. 5005–+, 2009.

[58] A. Domenichini, J. S. Edmands, A. Adamska, R. R. Begicevic, S. Paternoster, and M. Falasca, "Pancreatic cancer tumorspheres are cancer stem-like cells with increased chemoresistance and reduced metabolic potential," *Adv Biol Regul*, vol. 72, pp. 63–77, 2019.

[59] C. S. Ki, L. TY, M. Korc, and C. C. Lin, "Thiol-ene hydrogels as desmoplasia-mimetic matrices for modeling pancreatic cancer cell growth, invasion, and drug resistance." *Biomaterials*, vol. 35, no. 36, pp. 9668–9677, 2014.

[60] S. Uman, A. Dhand, and J. A. Burdick, "Recent advances in shear-thinning and self-healing hydrogels for biomedical applications," *Journal of Applied Polymer Science*, 2019.

[61] Y. L. Zhang, C. K. Fu, Y. S. Li, K. Wang, X. Wang, Y. Wei, and L. Tao, "Synthesis of an injectable, self-healable and dual responsive hydrogel for drug delivery and 3d cell cultivation," *Polymer Chemistry*, vol. 8, no. 3, pp. 537–544, 2017.

[62] C. Chen, S. Zhao, A. Karnad, and J. W. Freeman, "The biology and role of cd44 in cancer progression: therapeutic implications," *J Hematol Oncol*, vol. 11, no. 1, p. 64, 2018.

[63] C. S. Ki, H. Shih, and C. C. Lin, "Effect of 3d matrix compositions on the efficacy of egfr inhibition in pancreatic ductal adenocarcinoma cells," *Biomacromolecules*, vol. 14, no. 9, pp. 3017–26, 2013.